Near real-time PM1 chemical composition measurements at a French urban background and coastal site under industrial influence over more than a year: Temporal variability and assessment of sulfur-containing emissions

Shouwen Zhang, Emmanuel Tison, Sébastien Dusanter, Charles Beaugard, Cyril Gengembre, Patrick Augustin, Marc Fourmentin, Hervé Delbarre, Véronique Riffault

Near real-time PM_1 chemical composition measurements at a French urban background and coastal site under industrial influence over more than a year: Temporal variability and assessment of sulfur-containing emissions

Shouwen Zhang [1,2 *], Emmanuel Tison [1], Sébastien Dusanter [1], Charles Beaugard [3], Cyril Gengembre [2], Patrick Augustin [2], Marc Fourmentin [2], Hervé Delbarre [2], Véronique Riffault [1‡]

[1] IMT Lille Douai, Univ. Lille, SAGE - Sciences de l'Atmosphère et Génie de l'Environnement, F-59000 Lille, France

[2] Université du Littoral Côte d'Opale, Laboratoire de Physico-Chimie de l'Atmosphère, F-59140, Dunkerque, France

[3] Atmo Hauts de France, F-59000, Lille, France

* now at Atmo Hauts-de-France, F-59000, Lille, France

[‡] Correspondence to: Véronique Riffault (veronique.riffault@imt-lille-douai.fr)

Abstract

Near real-time measurements of submicron particulate matter (PM_1) were carried out at an industrial and coastal site in Dunkirk (Northern France) over a 14-month period (July 2013-September 2014). This site is surrounded by various industrial plants (metallurgy, petrochemistry, food processing, power plant, etc.) and is characterized by intense ship traffic (~700-800 per day along the English Channel) in harbour surroundings. The non-refractory (NR) submicron particles (organics, sulfate, nitrate, ammonium and chloride) and black carbon were measured by an Aerosol Chemical Speciation Monitor (ACSM) and an Aethalometer, respectively. Concomitant monitoring of CO_2, SO_2, and meteorological parameters was also performed. Both the seasonal (five seasons including two summers) and spatial (four identified sectors of emissions: marine, urban, industrial-urban and industrial) variabilities were investigated.

We present a descriptive analysis of the PM_1 composition, whose ambient concentrations ranged from less than 1 µg m^{-3} up to approximately 100 µg m^{-3} during a few pollution events. Gaseous SO_2 and particulate SO_4 were systematically observed at high concentrations (up to 310 and 48.2 µg m^{-3}, respectively) when industrial plumes reached the monitoring site. The conversion ratio of particulate (S_p) to total (S_{tot}) sulfur is relatively constant at 0.1 when RH ranges from 30-70% but reaches an average value of 0.3 at high RH (90-100%). This reflects an enhancement of SO_2-to-SO_4 gas-particle conversion processes resulting in an increase of aerosol acidity as shown by a comparison between measured and predicted NH_4 concentrations. An impact of the vertical mixing on the SO_2-to-SO_4 conversion was also observed using vertical turbulence (σ_w) as a descriptive parameter. Indeed, the conversion ratio (S_p/S_{tot}) was found to be reduced under high turbulence conditions due to dilution effects.

Keywords: ACSM, Aethalometer, Submicron particulate matter, Industrial area

1 Introduction

Atmospheric aerosols from both natural and anthropogenic sources have been widely studied during the last decades to assess their influence on climate. Indeed, their optical properties (light scattering and absorption) and their ability to act as cloud condensation nuclei (Flossmann et al. 1985, Ghan and Schwartz 2007) can significantly impact the Earth's radiative balance. In addition, aerosols can strongly impair human health (Pope et al. 2002, Kelly and Fussell 2012, Leclercq et al. 2017) and the wellbeing of ecosystems (Bouwman et al. 2002, Niyogi et al. 2004). Based on their ability to deposit in the respiratory tract, aerosols are classified as PM_{10}, $PM_{2.5}$, and PM_1, characterized by aerodynamic diameters lower than 10, 2.5 and 1 micrometers, respectively. The World Health Organization (WHO) estimates that $PM_{2.5}$ contributes to approximately 0.8 million deaths per year and ranked it as the 13th cause of global mortality (WHO 2002, Cohen et al. 2005, Elder et al. 2009). In the urban environment, PM_1 exhibits a stronger impact on human health than $PM_{2.5}$ since (i) they can penetrate further into the alveolar region, (ii) their chemical composition is dominated by anthropogenic sources and (iii) they lead to a more intense pro-inflammatory response (Pérez et al. 2008, Ramgolam et al. 2009, Kelly and Fussell 2012, Mazzarella et al. 2012).

Submicron non-refractory particulate matter (NR-PM_1) can be characterized at a high time resolution using Aerosol Mass Spectrometers (AMS) during short field campaigns over a few weeks. Details about both the chemical composition (organics, nitrate, sulfate, ammonium and chloride) and the size distribution at temporal resolutions of a few minutes have been obtained worldwide (Jayne et al. 2000, DeCarlo et al. 2006, Canagaratna et al. 2007, Zhang et al. 2007, Jimenez et al. 2009). However, despite the unique qualities of an AMS to provide chemical information on PM_1, this type of instruments exhibits several drawbacks for long-term monitoring, such as the need for frequent calibrations and highly skilled operators.

More recently, the Aerosol Chemical Speciation Monitor (ACSM) (Aerodyne Research, Inc.) was designed and proposed for long-term monitoring (Ng et al. 2011). In contrast to an AMS, ACSMs do not provide the particle size distribution and exhibit a lower mass resolution, which in turn leads to fewer details about the organic composition. However, ACSM instruments do not require frequent calibrations, are less expensive, and are easier to use during field measurements. It is interesting to note that AMS and ACSM instruments have been already compared several times. A 3-week campaign performed at Queens College (New York, USA) in 2010 showed good correlations (R^2 of 0.81–0.91, slopes of 0.76–1.01) between the two techniques for all measured species (organics, nitrate, sulfate, ammonium and chloride) (Ng et al. 2011). A larger scale intercomparison exercise involving 13 Q-ACSM

and one HR-ToF-AMS in Paris (Crenn et al. 2015) showed good agreements between the different instruments with R^2 values higher than 0.9, except for chloride, and slopes ranging from 0.62 to 1.43 depending on the species considered.

Industrial activities are important sources of anthropogenic Particulate Matter (PM) (Taiwo et al. 2014, Riffault et al. 2015). However, previous sampling sites where AMS and ACSM instruments have been deployed were usually located in urban, suburban or rural background regions and only a few were impacted by industrial emissions (El Haddad et al. 2013, Budisulistiorini et al. 2015). In Europe, industrial processes represent the third (9.1%) and second (28.6%) primary sources of $PM_{2.5}$ and PM_{10} (EEA 2015), respectively. In France itself, industrial sources accounted for 22% and 29% of $PM_{2.5}$ and PM_{10} in 2012, respectively (CGDD 2014). Of interest for the present study, the Hauts-de-France (HdF) region in France is still heavily industrialized, with industries contributing to 68 and 61% of $PM_{2.5}$ and PM_1 emissions, respectively, in the Dunkirk conurbation (AtmoHdF 2012).

Dunkirk, located in northern France, is impacted by industrial activities such as metallurgy, petrochemistry, food processing, power plant, etc., and is also the first energy platform in HdF. This industrial activity results in massive emissions of gaseous and particulate pollutants, including for the year 2011 Volatile Organic Compounds (VOCs; 1,556 tons), oxides of nitrogen (NO_x, 8,195 tons), sulfur dioxide (SO_2, 11,752 tons), and particulate matter (10 nm-100 µm; 3,246 tons) (DREAL 2012).

Previous studies focusing on particulate matter in Dunkirk have investigated concentrations in heavy metals (Alleman et al. 2010, Mbengue et al. 2014) and inorganic species (Rimetz-Planchon et al. 2008) in PM_{10}. The organic fraction has also been studied in $PM_{2.5}$ using offline filter methods (Cazier et al. 2011, Crenn et al. 2017, Crenn et al. 2018) and in PM_1 using an Aerosol Mass Spectrometer (AMS) (Crenn et al. 2017, Crenn et al. 2018, Setyan et al. 2019). PAHs (Polycyclic Aromatic Hydrocarbons) and sulfate in NR-PM_1 have been found almost exclusively in winter for air masses coming from the industrial zone. However, the filter methods required long sampling times (typically 24-72 hours), precluding any investigation of fast changes in aerosol composition and levels. The two campaigns employing an AMS were only performed for short periods (summer and winter, approximately 1 month each), with only a few wind occurrences from the industrial sector.

Volatile Organic Compounds (VOCs), considered as potential precursors of organic aerosols, have also been investigated in Dunkirk (Badol et al. 2008, Badol et al. 2008, Roukos et al. 2009). Badol et al. (2008) carried out a measurement campaign of about one year and identified 53 VOCs (Badol et al. 2008). Daily profiles, seasonal variations and pollution roses

observed for these compounds indicated strong impacts of traffic, solvent evaporation and industrial emissions on the measured concentrations. In addition, a Chemical Mass Balance (CMB) source-receptor model was applied to estimate the contributions of various emission sources, including 6 urban profiles and 7 industrial profiles (Badol et al. 2008). Roukos et al. (2009) carried out two measurement campaigns in summer and winter 2007 using passive sampling on adsorbent cartridges (Roukos et al. 2009). This study showed that pollution transported over long distances has a significant impact on VOC concentrations in the Dunkirk area during specific weather conditions. Xiang et al. (Xiang et al. 2012) reported a source apportionment study coupling a Positive Matrix Factorization (PMF) analysis and micro-meteorology observations. This study highlighted that an increase of the turbulence could lead to a lower contribution of ground level sources and an enhanced contribution of elevated sources (such as plumes from chimneys).

The present study provides the first near real-time and long-term (> 1 year) monitoring of submicron aerosols at an urban background and coastal site strongly impacted by industrial activities (within a few km). This work aims at better understanding PM_1 temporal variability in terms of mass concentration and chemical composition, and their transformation in this complex environment. Organic PM_1 sources will be further investigated using PMF in a forthcoming paper. The database of PM_1 measurements is analyzed by seasons and wind sectors to investigate the origin of local emissions. Particular attention was paid to the impact of industrial sulfur emissions on the formation of sulfate particles.

2 Experimental section

2.1 Campaign description

The measurement site was located on the eastern side of the Dunkirk harbour (Port-Est, PE: 51°3.12' N; 2°21.24' E; 1 m). This site is surrounded, within a few kilometers, by an intensive industrial zone at W-SW and by a residential zone at S-SE as shown in Figure 1. This geographical location allows classifying the origin of local air masses according to four wind sectors: marine (M; 271° -70°), urban (U; 71° - 140°), industrial-urban (IU; 141° - 225°), and industrial (I; 226° - 270°). This site can sometimes be under the influence of remote sources from France, Belgium, England, and Germany within a few tens to hundreds of kilometers.

The field campaign was conducted over 14 months from July 15, 2013 to September 10, 2014. An ACSM and an Aethalometer (described below) were installed at the PE site, alongside an SO_2 analyzer (AF21M, Environnement SA) managed by the Atmo HdF regional

air quality monitoring network and a CO_2 analyzer (VS-3000, HORIBA). The SO_2 analyzer was operated continuously at a time resolution of 15 min and was calibrated once a month using a SO_2 gas standard at 200 ppb (Air Liquide). The CO_2 analyzer was calibrated 3 times during the campaign, using a CO_2 gas standard at 997 ppm (purity > 99.9%, Praxair). An ultrasonic anemometer (uSonic-3 Scientific, METEK) was deployed at a nearby site approximately 1 km away (Figure 1) for measuring horizontal and vertical wind speeds and direction, as well as temperature and turbulence parameters. Standard meteorological parameters such as temperature, relative humidity, precipitation, pressure, and solar radiation were also recorded on the rooftop of a research building of the Université du Littoral Côte d'Opale (51°2.14'N; 2°22.05'E), located at 2 km. From June 23, 2014 to September 10, 2014, an ambient particulate monitor (TEOM-FDMS 1405-F, Thermo Fischer Scientific) was additionally deployed to measure the total PM_1 mass concentration. Section A of the Supplementary Information reports the number of valid data (Table S1) as well as the temporal data coverage (Figure S1) for each instrument. Measurements were averaged over the ACSM time stamp using Coordinated Universal Time (UTC).

2.2 PM_1 chemical composition

2.2.1 Aerosol Chemical Speciation Monitor (ACSM)

The ACSM (Aerodyne Research Inc.) provides measurements of particulate organics, nitrate, sulfate, ammonium and chloride in the non-refractory submicron particles (Ng et al. 2011). The aerodynamic lens inside the ACSM inlet sampled PM_1 at a flow rate of approximately 80 $cm^3\ min^{-1}$, controlled by a 100 µm diameter critical aperture. Non-refractory components were vaporized at 600°C after impaction on an inverted-cone surface and then ionized by electron impact at 70 eV. A RGA (residual gas analyzer) quadrupole mass spectrometer was used to acquire mass spectra at a mass resolution of one unit and up to 148 amu. During acquisition, the ACSM was operated with a three-way automatic valve to switch between the filter mode (particle-free air) and the sample mode (ambient air). The difference between these two modes is considered as the signal generated by ambient aerosols. The scan speed was set to 200 ms amu^{-1}. 28 scans were acquired for both the filter and the sample modes, resulting in a time resolution of approximately 30 min. The instrument was installed in an air-conditioned room (20°C) for continuous monitoring.

Ambient aerosols were sampled through a $PM_{2.5}$ cyclone (URG-2000-30EQ) at a flow rate of 3 L min^{-1} and a stainless-steel tube whose length and inner diameter were 2.1 m and 1.27 cm, respectively (residence time in the sampling tube was approximately 5 seconds). The particle

size-dependent loss due to the sampling setup was calculated using the Particle Loss Calculator (PLC) (von der Weiden et al. 2009), and was found to be negligible (< 1%). Sampled aerosols were dried using a Nafion dryer (PD-200T-12 MPS, Perma Pure) reaching a relative humidity (RH) always lower than 30%, which is important to minimize the effect of RH on the collection efficiency (CE) as discussed later in this section.

The mass spectra acquired by ACSM were analyzed using a fragmentation table (Allan et al. 2004, Canagaratna et al. 2007) to extract distinct chemical species or group of species. The mass concentration of a species *s* (C_s) is derived from the measured ion current $IC_{s,i}$ (amperes) using Equation (1):

$$C_s = \frac{CE_s}{T_{m/z}} \times \frac{10^{12}}{RIE_s} \times \frac{Q_{cal} \times G_{cal}}{RF_{NO_3}} \times \frac{1}{Q \times G} \sum_{alli} IC_{s,i} \quad (1)$$

where $\Sigma IC_{s,i}$ is the sum of the ensemble mass spectrum fragment i contributing to species s; CE_s is the collection efficiency of a species *s* ; $T_{m/z}$ the ion transmission efficiency; RF_{NO3} (ions/molecule) the response factor for NO_3; and RIE_s the relative ionization efficiency of a species s compared to NO_3; Q_{cal} and G_{cal} are the volumetric sample flow rate ($cm^3\ s^{-1}$) and multiplier gain (~ 20,000) measured during calibrations of RF_{NO3}, respectively. In general, values of Q and G observed during ambient measurements are similar to the values measured during calibration experiments (Q_{cal} and G_{cal}) and these parameters cancel out in Eq. (1).

The instrument calibration protocols and signal optimization are based on existing procedures (Ng et al. 2011) and are presented in more details in the Supplementary Information (section B). The NO_3 response factor (RF_{NO3}) and the relative ionization efficiency (RIE_s) were calibrated at the beginning and periodically during the campaign (once per month). Average values of RF_{NO3} (3.81×10^{-11}) and RIE_s (NH_4: 5.67; SO_4: 0.55; Cl: 2.26) were used for the whole campaign. For organics, the default value of RIE(1.4) was used (Jimenez et al. 2003). The RF_{NO3} and RIE_{NH4} values observed in the present study are close to the average value of 13 Q-ACSM used during the intercomparison exercise described by Crenn et al. (Crenn et al. 2015), i.e. 3.55×10^{-11} and 6.31, respectively. Most previous studies used the default values of 1.2 for SO_4 (Ng et al. 2011) and 1.3 for Cl (Alfarra et al. 2004) but RIE(SO_4) has been found to vary from one instrument to another (Ng et al. 2011).

The CE of a species *s* is mainly influenced by particle humidity (for RH > 80%), acidity, and the mass fraction of ammonium nitrate (Matthew et al. 2008). Humidity effects are ignored in the present study because particles were dried at RH below 30%. However, both particle acidity and the fraction of ammonium nitrate were taken into consideration for the calculation

of CE, using the method described by Middlebrook et al. (Middlebrook et al. 2011) and described in the Supplementary Information (section C) where the CE time series can be found (Figure S1). More than 57% of the CE values were at 0.45 and the rest ranged from 0.45-0.9 during the campaign.

As the ACSM is equipped with a quadrupole mass spectrometer, the m/z-dependent ion transmission efficiency ($T_{m/z}$) is assessed using an internal naphthalene standard whose parent ion is detected at m/z 128 and several fragments are detected at lower m/z. Finally, a reference period was chosen when the signal of air beam (m/z = 28, corresponding to N_2^+) is stable and as close as possible to 10^{-7} A. This normalization takes into account the variation of air beam over time, as well as the changes in the detector sensitivity and flow rate.

ACSM data were acquired using ACSM_DAQ_v1438 at a time resolution of 30 min and processed using ACSM_Local_v1535 (ARI) with Igor Pro 6.36 (WaveMetrics, Inc., Oregon USA). A total of 15,231 valid observations was recorded, split as follows between the four wind sectors: M − 5,527 (36%), U − 1,257 (8%), IU − 6,590 (43%) and I − 1,857 (12%).

2.2.2 Aethalometer

Black carbon was measured with a two-wavelength aethalometer (AE42, Magee Scientific Inc.) at 880 nm. The aethalometer sampled ambient air at a flow rate of 5 liters per minute through a PM_1 sampling head (SCC-1.197, BGI). Samples were collected at a time resolution of 5 min on a moving tape made of quartz fibers. The tape does not move forward until the spot reaches a certain density (set at 60% in this study). The principle of the aethalometer is to measure the optical attenuation of the collected aerosols and the BC concentration is calculated from the attenuation variation at a wavelength of 880 nm:

$$BC_{raw} = \frac{A \times \Delta ATN}{\sigma_{ATN} \times Q \times \Delta t} \qquad (2)$$

where A is the surface of the sampling area on the filter (1.67 cm^2), Q the volumetric flow rate and ΔATN the variation of the attenuation during the time interval Δt. σ_{ATN} (m^2 g^{-1}) is the specific attenuation coefficient for BC.

However, according to the literature (Virkkula et al. 2007, Park et al. 2010), the relationship between the change in attenuation and BC concentration is not always linear. BC concentrations have been corrected using a procedure proposed by Weingartner et al. (Weingartner et al. 2003) as shown in Eq. (3):

$$BC_{corr} = BC_{raw} \times \frac{1}{C_{ref} \times \left(\frac{1}{m(1-\omega_0)+1} - 1 \right) \times \frac{\ln(ATN) - \ln(10\%)}{\ln(50\%) - \ln(10\%)} + 1} \quad (3)$$

where BC_{raw} is the concentration measured by the aethalometer from Eq. (6). C_{ref} and m values of 2.14 and 0.87, respectively, were used in the present study (Petzold et al. 1997, Weingartner et al. 2003). ω_0, the single scattering albedo (SSA) of the sampled aerosols, was taken from AERONET (AErosol RObotic NETwork, http://aeronet.gsfc.nasa.gov) measurements in Dunkirk (N 51°2.1', E 02°22.07') and an average value of 0.9 was used.

2.2.3 Wind and trajectory analyses

The wind and trajectory analyses combine the observed concentrations with wind and air mass conditions, in order to understand the origin of some pollutants, as described in more details in (Boichu et al. 2019) and (Roig Rodelas et al. 2019). Briefly, these analyses were performed using the Zefir tool v.3.70 (Petit et al. 2017). We used (i) the non-parametric wind regression (NWR) model to study the regional vs. local origin of a given pollutant based on local wind speed and direction provided by the ultrasonic anemometer; and (ii) the Concentration-Weighted Trajectory (CWT) method to determine the regions of emissions for transported ammonium and nitrate and/or their precursors, using backtrajectories calculated with HYSPLIT 4 and meteorological data from the Global Data Assimilation System (GDAS) at 1°×1° spatial resolution (Stein et al. 2016). 3-day backward trajectories arriving at 500 m above ground level were calculated every 6 hours over the whole campaign.

3 Results and discussion

3.1 Meteorology

Time series of meteorological parameters are displayed in Figure 2 and their seasonal variability is reported in Table 1. The maximum solar radiation varied roughly from 300 (winter) to 800 W m^{-2} (summer). The seasonal ratio of maximum to mean radiation indicates the impact of cloud coverage. Cloud coverage is on average similar in spring-summer and autumn-winter periods, but the ratio increases by about 50% in autumn and wintertime. Over the whole campaign, pressure and temperature time series are also displayed, with average values of 1013 hPa and 14°C, varying from 978 to 1037 hPa and from 1.4 to 32.2 °C, respectively. The average wind speed was 4.9 m s^{-1}, with higher values during fall (5.3 m s^{-1}) and winter (5.9 m s^{-1}), and lower values during spring (4.7 m s^{-1}) and summer

(4.2 m s^{-1}). Seasonal mean and maximum pressures indicate clearly an increase of the frequency of low pressure systems in autumn and winter, corresponding to south-southwesterly winds from the North Atlantic Ocean.

The winter season was mild in 2013-2014, with no frost, but high wind speed events (>14 m s^{-1}) were observed during 12 days from October to February, including 5 remarkable storms (Christian, Godehard, Xaver, Dirk and Qumara). The summer was also mild with moderate temperatures (20-25°C) due to the proximity of the North Sea, and the development of 18 sea-breeze events. During low wind speed periods, 14 fog events occurred. Rain (> 1 mm/hour) was observed on 51 days, enhancing wet deposition mechanisms of particles.

Figure S3 (section D of the SI) shows the seasonal variation of the distribution (normalized to 100%) of sectorial winds according to previously defined ranges of wind directions. The marine sector exhibited the strongest seasonal variation, with a contribution to the wind distribution during summers 2013 and 2014 higher than 50% but reduced to ~20% during winter. The urban sector exhibited a small contribution of ~10% during the whole campaign. However, even with such a small contribution, air masses originating from this sector can bring high PM concentrations to the measurement site (see next section). The industrial sector also exhibited a constant contribution of approximately 10%, independent of the season. The industrial-urban sector exhibited a larger contribution ranging from 30 to 70% all along the campaign, especially in winter when southern winds were observed. It is important to note that the seasonal variability of the wind distribution will be one of the main parameters driving PM_1 mass and composition variations.

Table 1. Mean, maximum and minimum values of the main parameters and chemical species for each season during the entire campaign

		Summer 2013	**Autumn 2013**	**Winter 2013-2014**	**Spring 2014**	**Summer 2014**
Wind speed	mean±σ	4.2 ± 2.0	5.3 ± 2.5	5.9 ± 2.5	4.7 ± 2.3	4.2 ± 2.0
(m s^{-1})	max	12.8	19.1	17.6	12.6	13.7
Radiation*	mean;	296;	132;	149;	306;	291;
(W m^{-2})	max	968	629	706	982	912
Pressure	mean±σ	1018 ± 7	1016 ± 11	1006 ± 12	1015 ± 8	1013 ± 5
(hPa)	min-max	993 - 1032	980 - 1037	978 - 1032	999 - 1036	995 - 1023
RH	mean±σ	79 ± 11	83 ± 7	83 ± 8	78 ± 11	79 ± 11
(%)	min-max	36 - 96	55 - 98	34 - 100	35 - 97	29 - 96
T	mean±σ	18.4 ± 2.5	11.8 ± 3.8	9.8 ± 2.4	13.7 ± 3.1	18.4 ± 2.2
(°C)	min-max	11.3 - 32.2	1.4 - 21.2	2.6 - 19.2	4.5 - 25.1	11.9 - 32.1
Precip.	mean±σ	0.01 ± 0.14	0.03 ± 0.15	0.03 ± 0.13	0.01 ± 0.11	0.02 ± 0.27
(mm/hour)	max	5	3.4	2.6	4.8	16
SO_2	mean±σ	11 ± 26	8 ± 19	11 ± 22	12 ± 20	10 ± 20

(µg m^{-3})	max	310	218	206	206	220
CO_2	mean±σ	430 ± 15	428 ± 16	414 ± 11	416 ± 14	415 ± 12
(ppm)	min-max	391 - 557	364 - 555	367 - 548	370 - 537	388 - 549
BC**	mean±σ	0.7 ± 0.8	/	0.8 ± 0.8	0.6 ± 0.9	0.5 ± 0.6
(µg m^{-3})	max	15.3	/	27.7	28.3	21.7
Org	mean±σ	2.0 ± 1.8	3.8 ± 5.1	3.3 ± 3.2	3.1 ± 3.0	2.4 ± 2.1
(µg m^{-3})	max	11.8	51.9	70.0	25.2	45.8
SO_4	mean±σ	2.9 ± 3.1	2.2 ± 2.8	1.8 ± 3.6	2.5 ± 2.8	2.5 ± 2.5
(µg m^{-3})	max	28.4	23.9	48.2	21.7	31.6
NO_3	mean±σ	1.3 ± 2.4	2.7 ± 4.0	2.5 ± 3.7	4.1 ± 4.7	1.6 ± 2.6
(µg m^{-3})	max	15.0	23.0	27.3	21.5	16.2
NH_4	mean±σ	1.1 ± 1.1	1.4 ± 1.7	1.2 ± 1.7	1.9 ± 1.6	1.1 ± 1.1
(µg m^{-3})	max	6.1	10.0	21.4	8.0	8.0
Cl	mean±σ	0.03 ± 0.07	0.09 ± 0.16	0.06 ± 0.10	0.06 ± 0.12	0.02 ± 0.04
(µg m^{-3})	max	1.5	3.2	2.3	2.0	0.7

* Radiation represents daytime values computed using only data after sunrise and before sunset.

** BC values are not available in autumn.

3.2 PM_1 mass concentration and chemical speciation

To check the aerosol measurements quality, the total mass concentration of PM_1 measured by the ACSM (NR-PM_1) and the aethalometer (BC) was compared to TEOM-FDMS measurements from June 23 to September 10, 2014 (Figure 3). Figure 3 displays time series of PM_1 from both (i) the ACSM and aethalometer and (ii) the TEOM-FDMS. This figure shows that PM_1 concentrations ranged from less than 1 µg m^{-3} to approximately 50 µg m^{-3} during the 2.5 months of the comparison period, with both traces showing similar temporal variations. A scatter plot of the ACSM + aethalomether and TEOM-FDMS measurements is shown in Figure 3b. This figure also displays 24-hour averaged values for both measurements, which indicate an excellent agreement (slope: 0.94; r^2 = 0.94), suggesting that (i) most of the PM_1 mass (7.9 ± 7.1 µg m^{-3} measured by the TEOM-FDMS) is captured by the combination of ACSM and aethalometer (8.1 ± 6.3 µg m^{-3}); (ii) the RF/RIE calibrations and the CE correction applied for the ACSM data analysis are correct within measurement uncertainties.

Time series of Cl, NH_4, NO_3, Organics and SO_4 measured by ACSM, and black carbon measured with the aethalometer, are displayed in Figure 4. Each species exhibits different temporal variations and concentration levels. Chloride is a minor fraction of PM_1 and its concentration is lower than 3 µg m^{-3} over the entire observation period. NH_4 is relatively constant throughout the whole year at levels lower than 5 µg m^{-3}, with the exception of spring 2014 (March-May) where levels up to 15 µg m^{-3} were observed. NO_3, Organics, SO_4 and BC are much more time-dependent, with concentrations rising to 30-50 µg m^{-3}.

Some PM_1 species seem to exhibit significant seasonal variations (Figure S4, section D of the SI; and Table 1). Average seasonal chloride concentrations were very low (< 0.1 µg m^{-3}).

Sulfates did not exhibit seasonal variations due to its industrial origin and showed similar contributions from this sector (wind occurrences) for all seasons. Nevertheless, the NWR plot (section E of the SI, Figure S5a) for sulfate shows a strong contribution from local sources, highlighting the industrial sector, and a minor one from the marine sector, which could be the result of ship emissions. This pattern is even more pronounced for its precursor SO_2 (Figure S5b) whose high concentrations are clearly pointing at the industrial area. For the other species, PM_1 measured during both summers 2013 and 2014 exhibit similar chemical compositions due to similar wind patterns, which in turn likely imply the impact of similar sources on the measurement site. However, the relative contribution of NO_3 is higher during cold seasons (autumn, winter and spring) compared to the two warmer summers (Table 1). Especially in spring 2014, NO_3 exhibits the highest average concentration (4 µg m^{-3}) and contribution (33%) when NH_3 emissions – required for the formation of ammonium nitrate – start to peak in North-Western Europe due to fertilizer spreading. Besides, whereas 96% of NH_3 emissions is attributed to the agricultural sector when considering the entire Hauts-de-France region, it decreases down to 50% in the Dunkirk area, where local emissions from the "manufacturing industries, waste treatment and construction" account for half according to the latest available inventory (AtmoHdF 2012). The levels of ammonium and nitrate could indeed be related to both a local and regional origin through their NWR plots (section E of the SI, Figure S5c and d). The regional influence was further investigated through Concentration-Weighted Trajectory (CWT) maps (section E of the SI, Figure S6), and pointed out a significant contribution from medium- to long-range transport of aged ammonium nitrate aerosols or their precursors from Central Europe (Germany, Poland, and Austria) (Figure S5). Organics concentrations and contributions are also higher during cold seasons (autumn and winter), which seems due to both local and regional sources (Figure S5e) coming from the industrial-urban sector (55-63% of wind occurrences), such as emissions from urban sources such as residential heating and traffic, while an additional contribution from industrial emissions in this direction (storage facility of petrochemical products and food processing industries) cannot be excluded. BC represents 5 to 9% of PM_1 mass but no clear observation is found for its seasonal variation.

For the sake of comparison with other studies, Figure 5 displays 17 field campaigns performed worldwide to investigate the composition of ambient aerosols. These studies employed ACSM instruments in different environments classified as urban (5 sites), suburban (2 sites), industrial-urban (2 sites) and rural (8 sites). For similar types of sites the studies are sorted by decreasing NR-PM_1 mass concentrations. The durations of these campaigns are

highly variable and range from 3 weeks to 7 years. Campaigns performed on a timescale of years can provide seasonal and even annual variations of submicron aerosols. The averaged mass concentration varies from approximately 2-6 µg m^{-3} for background sites (Hyytiälä, Montsec, Look Rock) (Budisulistiorini et al. 2015, Minguillón et al. 2015, Heikkinen et al. 2020) up to 30-50 µg m^{-3} for polluted cities (Santiago, Beijing) (Sun et al. 2012, Carbone et al. 2013). Our study indicates an annual concentration of 9.0 µg m^{-3}, which is similar to that observed for another industrial-urban site in Atlanta (9.5 µg m^{-3}) (Budisulistiorini et al. 2015), whose duration was one year.

The contribution of each species to NR-PM_1 is shown in the bottom panel of Figure 5. Organics dominate (> 50%) for most of the sites and the contribution can reach up to 70% as seen in Atlanta. In our study, organics account for 32% on average, which is within the lowest contributions observed worldwide and similar to that found at the SIRTA suburban site near Paris (39%) (Petit et al. 2015). Ammonium exhibits a relatively constant fraction at all locations, with an average value of approximately 12%. The sulfate component contributes from 8 to 35% of NR-PM_1, with higher contributions found for rural sites without (Tibetan Plateau: 30%; South Africa: 32%) (Tiitta et al. 2014, Du et al. 2015) or with urban influence (Senegal: 35%) (Rivellini et al. 2017). Interestingly, industrial sites do not exhibit the highest levels of sulfate, whose contribution to the chemical composition does not seem to depend on the nature of the site. Nitrate varies from 6% to 28%, with the highest values observed for Paris (28%) (Petit et al. 2015), Dunkirk (26%) (this work) and Beijing (25%) (Sun et al. 2012). Higher levels of NO_x (NO and NO_2) in urban areas are likely the cause for higher nitrate levels in PM_1 since NO_x are oxidized to nitric acid in the atmosphere, which in turn forms secondary nitrate particles (Matsumoto and Tanaka 1996). Chloride is always a minor fraction and represents less than 3% at all sites.

Figure 6 shows PM_1 mass concentrations and chemical compositions averaged over the entire campaign for the four wind sectors defined above (marine, urban, industrial and industrial-urban). The average concentration for all sectors is 9.4 ± 9.1 µg m^{-3} with significantly higher concentrations for the industrial (11.7 ± 8.8 µg m^{-3}) and urban (15.6 ± 9.5 µg m^{-3}) sectors, and a lower concentration for the marine sector (8.0 ± 8.5 µg m^{-3}). The organic fraction contributes from 28% up to 38% of the PM_1, with the exception of the industrial sector for which the aerosol composition is enriched in sulfate (only 14% organics). As mentioned before, a higher organic fraction for the industrial-urban sector could be due to a storage facility of petrochemical products or food processing industries in this area. For inorganic species, the ammonium contribution is similar between all sectors (≈14%) and non-refractory

chloride (therefore non-marine) represents less than 1% of the mass concentration. For chloride, the small but significantly higher contribution from the industrial sector reflects the presence of sources already identified in other campaigns in this area or similar ones (Hleis et al. 2013, Taiwo et al. 2014, Crenn et al. 2017, Setyan et al. 2019), e.g. the formation of KCl in the steelwork sintering process. Nitrate and sulfate contributions are more variable between the different sectors, with contributions ranging from 8-35% for NO_3 and 13-58% for SO_4. The urban and industrial sectors stand out by exhibiting the highest contributions for nitrate (about 35%) and sulfates (about 58%), respectively. As mentioned previously, these higher contributions may be due to higher NO_x and SO_2 emissions in the urban and industrial sectors, respectively. BC contributes about 5% for the marine and industrial sectors, while it reaches 8 to 9% for the urban and industrial-urban sectors where traffic and wood burning may be significant sources.

3.3 Aerosol ion balance

To investigate the ion balance of the sampled aerosols, a predicted concentration of NH_4 was calculated from the sum of chloride, nitrate and sulfate ion concentrations using Eq. (2). These ions are assumed to be bound to ammonium in a neutral aerosol to form NH_4Cl, NH_4NO_3 and $(NH_4)_2SO_4$, respectively. The calculated value ($NH_{4,predicted}$) is then compared to the measured NH_4 concentration. If the two values are similar, the particles are fully neutralized. Although an ion balance cannot be used as a direct measurement of pH in aerosols, it can still be used to distinguish qualitatively between an "acidic" (negative balance; below the 1:1 line) and an "alkaline" (positive balance; above the 1:1 line) aerosol (Zhang et al. 2007, Guo et al. 2015).

Particles are considered "more acidic" if the measured concentration is lower than the predicted value, since the imbalance indicates that acidic compounds such as H_2SO_4, HNO_3 or HCl are likely present in the aerosol. Note that as Cl being a minor fraction (<1%) of NR-PM_1, the contribution of HCl to the aerosol ion balance − if present − is negligible.

Figure 7 displays the correlation between measured and predicted NH_4 with a color coding based on SO_4 concentrations. All SO_4 concentrations higher than 25 µg m^{-3} are included in the red color. When the symbols are scattered around the 1:1 line, the measured and predicted concentrations are in good agreement, indicating that particulate ammonium is fully neutralized. When the symbols are significantly below the 1:1 line, there is an overestimation of the predicted concentrations. As mentioned above, this overestimation may be due to either

a lack of ammonium (thus of NH_3) or the presence of acidic species in the particles, which may be characteristic of "fresh" emissions.

Aerosols appear not neutralized or “acidic” (below the 1:1 line) with high sulfate concentrations (Figure 7a) but not with high nitrate concentrations (Figure S7, section F of the SI). This observation suggests that aerosol ion balance is driven by acidic sulfate compounds. The same analysis is displayed for the four wind sectors in Figure 7b-e. For the marine and urban sectors, the aerosols are well neutralized and SO_4 concentrations are low (4-5 $\mu g\ m^{-3}$ on average). NH_4 is therefore mainly bound to NO_3. The industrial sector shows strong deviations from the 1:1 line, with higher acidity levels correlated to elevated SO_4 concentrations (Figure 7e), which suggests that acidic aerosols are due to “fresh” industrial emissions of sulfur compounds. It is interesting to note that the industrial-urban sector shows a mixed behavior between industrial and urban sectors.

In order to investigate the influence of acidity on the NR-PM_1 composition, the measured-to-predicted NH_4 ratio was plotted as box plots for the entire campaign and the four sectors in Figure 8a. The aerosol composition for acidic and non-acidic particles is displayed in Figure 8b. Figure 8a clearly shows that the industrial sector exhibits the lowest $NH_{4,measured}$-to-$NH_{4,predicted}$ ratio (0.64 on average), corresponding to the most acidic particles (ratio threshold of 0.75). This ratio can be seen as a rough indicator of an equal number of moles of $(NH_4)_2SO_4$ and NH_4HSO_4 (Zhang et al. 2005). The neutralized particles were defined for a ratio ranging from the mean value of 0.85 to the 90^{th} percentile (1.07). The “most acidic” and “neutralized” periods account for 22% and 41% of the total sampling time, respectively. The rest of the observations falls into a mildly acidic regime and are not analyzed separately. Figure 8b displays the average composition of “neutralized” and “most acidic” particles, respectively. Compared to those considered as neutralized, the “most acidic” particles represent only half the mass. However, they contain more SO_4 (58% compared to 17%), which is consistent with the above discussion. The acidic particles contain less nitrate (7% compared to 34%), probably due to the displacement of HNO_3 by H_2SO_4 in the competition for NH_3 (West et al. 1999).

3.4 SO_2-to-SO_4 conversion

In the absence of direct measurements of industrial emissions, it is likely that some of the particulate sulfate is directly produced during industrial processes, in particular as by-products of the coke oven used to feed the three blast furnaces of the main steelworks in the area. Furthermore, NH_4HSO_4 could be formed at the exit of the chimneys through the direct

441 reaction of SO_3 with H_2O and NH_3 in the presence of additional molecules (Chen et al. 2018).
442 Then NH_4HSO_4 can quickly react with NH_3 and form ammonium sulfate. However, a rapid
443 conversion of gaseous SO_2 into particulate sulfate could also contribute to the large sulfate
444 concentrations observed at the measurement site when the wind originates from the industrial
445 sector. The conversion can take place both in the gas phase (Stockwell and Calvert 1983,
446 Atkinson and Lloyd 1984) through an oxidation of SO_2 initiated by OH radicals, and in the
447 aqueous phase through reactions involving H_2O_2 and O_3 (Jacob and Hoffmann 1983,
448 Schwartz 1987). The sulfuric acid thus generated has a strong ability to nucleate in the
449 presence of water molecules and to form new particles by condensation of other low volatility
450 species (Kulmala et al. 2000, Weber et al. 2001). However, the oxidation of SO_2 in aqueous
451 phase is faster than in the gas-phase (Khoder 2002). Eatough et al. (1994) found that the gas-
452 phase oxidation rate can vary from <1% to 10% of ambient SO_2 per hour at high temperature
453 and relative humidity. Meanwhile, in the aqueous-phase the rate can reach 100% of SO_2
454 converted in less than an hour under optimum conditions (Eatough et al. 1994). Other
455 pathways such as the heterogeneous oxidation of S(IV) catalyzed by Fe(III) or Mn(II) (Jacob
456 and Hoffmann 1983) can occur, especially in this area where heavy metals have been
457 evidenced as important tracers of industrial emissions (Alleman et al. 2010, Setyan et al.
458 2019): When sulfuric acid is formed within or transferred to the aerosol, it reacts easily with
459 gaseous ammonia to form ammonium sulfate at the particle surface (Matsumoto and Tanaka
460 1996).
461 The observation of industrial plumes arriving at our ground sampling site requires that two
462 simultaneous conditions are met: (i) wind blowing from the southwest (industrial direction);
463 (ii) unstable atmospheric conditions favoring the dispersion of the plume. The Non-parametric
464 Wind Regression (NWR) plots of gaseous SO_2 and particulate SO_4 (Figure S6, a and b)
465 confirm that high concentrations observed at the receptor site are mainly originating from the
466 industrial sector (226°- 270°). Similar results were observed by a recent study near steel
467 plants in China, which showed important increases in sulfate, ammonium, CO and SO_2 when
468 industrial plumes reached the sampling site (Lei et al. 2020).
469 To assess whether the conversion of SO_2 into SO_4 was of importance during this study, the
470 influence of several microphysical and meteorological parameters on SO_2, SO_4 and the
471 particulate sulfur fraction has been investigated. These parameters included atmospheric
472 vertical turbulences via the standard deviation σ_w of vertical wind speed w, horizontal wind
473 speed, relative humidity and temperature.

We defined the particulate sulfur fraction as the ratio of particulate sulfur to total sulfur (S_p/S_{tot}), which is calculated as:

$$\frac{S_p}{S_{tot}} = \frac{[SO_4]\times\frac{32}{96}}{[SO_2]\times\frac{32}{64}+[SO_4]\times\frac{32}{96}} \quad (4)$$

S_p/S_{tot} only takes into account the sulfur content and is not influenced by the oxygen content. Two key parameters (RH and vertical turbulence) were found to significantly influence the gas-particle partitioning of sulfur as shown in Figure 9 (left and right, respectively). SO_2 and SO_4 concentrations, as well as S_p/S_{tot} ratios, shown in this figure are only considered within the industrial sector to focus on the SO_2-to-SO_4 conversion that occurs on a short timescale (4-30 min) during the transport of fresh industrial emissions of sulfur compounds to the sampling site. This data was binned accordingly to the descriptive parameter (RH, σ_w) with the number of observations for each bin shown at the top of the first panel.

Figure 9a shows that SO_2 increases linearly with relative humidity until 70-80%. This concomitant increase in RH and SO_2 could be due to industrial plumes passing over the measurement site since these plumes are likely emitted with large concentrations of both water and SO_2. Interestingly, the SO_2 concentration starts decreasing when RH is higher than 80%, but an opposite trend is observed for SO_4 (Figure 9b). Indeed, SO_4 also increases with RH until 80% but does not decrease for higher humidity levels. This behavior could be related to a higher rate of SO_2 conversion at high humidity. In Figure 9c, the S_p/S_{tot} ratio clearly shows that the particulate sulfur fraction is almost constant (approximately 0.1 with a low level of dispersion in the values) for low RH conditions (RH < 70%). However, the sulfur content is shifted from the gaseous to the particulate phase when RH is higher than 70-80% (S_p/S_{tot} increases to 0.3 at 90-100% RH). This is likely due to the gas-particle conversion that is favored under high RH conditions when the fast aqueous phase oxidation dominates. Sun et al. reported a similar impact of RH on sulfate aerosols in Beijing for the winter season (Sun et al. 2013). The authors showed that the average SO_4-to-total sulfur ratio is less than 0.05 at low RH (< 40%), indicating a very low sulfur oxidation ratio. This ratio quickly increases and reaches 0.23 at high RH (80-90%). Recently, Zhao et al. studied the conversion of SO_2 into sulfates on soot surfaces and found that water promotes sulfate formation for RH ranging from 6%–70%, while RH > 80% inhibits it (Zhao et al. 2017). This trend was not observed here because BC is only a minor contributor (~7%) of PM_1.

The atmospheric vertical turbulence can be characterized by the standard deviation σ_w of the vertical wind speed w. This metric represents the fluctuation of vertical wind speed in units of m s^{-1} and quantifies the vertical mixing of air masses within the surface layer. Trends in SO_2,

SO_4 and S_p/S_{tot} on this parameter are shown in Figure 9 (right). For both SO_2 and SO_4, higher σ_w values lead to higher concentrations (Figure 9a-b). As previously discussed, this can be explained by elevated emission sources such as plumes from industrial chimneys, which can reach the ground surface after dispersion only with strong enough vertical mixing. This behavior had already been observed for some VOCs at the same site (Xiang et al. 2012). In contrast, S_p/S_{tot} decreases with σ_w (Figure 9c), which suggests that the SO_2-to-SO_4 conversion is less favored under highly turbulent conditions.

To better understand the multi-influence of humidity and vertical turbulence (σ_w) on the conversion process, the examination of the RH dependence of the S_p/S_{tot} ratio was carried out using four bins of σ_w (0-0.5, 0.5-1, 1-1.5 and ≥1.5 m s^{-1}) (Figure S7). This shows that the S_p/S_{tot} ratio increases significantly with RH for each σ_w bin, except for the last one ($\sigma_w \geq 1.5$ m s^{-1}) where the change is unclear. Interestingly, higher conversion ratios seem to be observed for low values of σ_w, which may be due to lower wind speed values, and as a consequence, longer conversion times between the emission source and the measurement site. These results indicate that high RH (> 70%) and relatively low σ_w values (< 1 m s^{-1}) are the best conditions for an efficient SO_2-to-SO_4 conversion at this site.

4 Conclusions

The first long-term and near real-time measurements of the chemical composition of submicron aerosols at an urban background and coastal site impacted by industrial emissions showed a unique chemical signature compared to previous datasets existing in the literature. The aerosol evolution and processing are tightly linked with meteorology and even micrometeorology due to the complex dynamics of coastal areas, and the industrial emissions at various stack heights. The complete dataset has been analyzed according to the season and four different wind sectors. The aerosol ion balance based on measured and predicted NH_4 suggests that the majority of the particles are neutralized in the marine and urban sectors, whereas in the industrial sector, “more acidic” particles generally contain significantly higher concentrations of sulfate (~60%). Gas-phase SO_2 is strongly emitted in the nearby industrial area and quickly processed to form secondary SO_4 particles on a timescale shorter than 30 min. Both SO_2 and SO_4 were mostly emitted by chimneys and therefore influenced by atmospheric vertical mixing. High RH (>70%) and relatively low σ_w values (< 1 m s^{-1}) provided the best conditions for an efficient SO_2-to-SO_4 conversion rate.

Acknowledgements

IMT Lille Douai and LPCA acknowledge financial support from the CaPPA (Chemical and Physical Properties of the Atmosphere) project funded by the French National Research Agency (ANR) through the PIA (Programme d'Investissement d'Avenir) under contract ANR-11-LABX-0005-01, and two CPER projects funded by the French Ministry of Higher Education and Research, the CNRS, the Regional Council "Hauts-de-France" and the European Regional Development Fund (ERDF): Climibio, and IRENI (additionally financed by the Communauté Urbaine de Dunkerque). We thank P. Goloub (LOA, Univ. Lille) for his efforts in establishing and maintaining the PHOTONS/AERONET network, and L. Paringaux (Atmo HdF) for technical support throughout the campaign. S. Zhang thanks IMT Lille Douai and the Regional Council "Hauts-de-France" for her PhD grant. A. Chakraborty (IMT Lille Douai) is acknowledged for helpful discussions.

References

Alfarra, M. R., H. Coe, J. D. Allan, K. N. Bower, H. Boudries, M. R. Canagaratna, J. L. Jimenez, J. T. Jayne, A. A. Garforth, S.-M. Li and D. R. Worsnop (2004). "Characterization of urban and rural organic particulate in the Lower Fraser Valley using two Aerodyne Aerosol Mass Spectrometers." Atmospheric Environment **38**(34): 5745-5758.

Allan, J. D., A. E. Delia, H. Coe, K. N. Bower, M. R. Alfarra, J. L. Jimenez, A. M. Middlebrook, F. Drewnick, T. B. Onasch, M. R. Canagaratna, J. T. Jayne and D. R. Worsnop (2004). "A generalised method for the extraction of chemically resolved mass spectra from Aerodyne aerosol mass spectrometer data." Journal of Aerosol Science **35**(7): 909-922.

Alleman, L. Y., L. Lamaison, E. Perdrix, A. Robache and J.-C. Galloo (2010). "PM10 metal concentrations and source identification using positive matrix factorization and wind sectoring in a French industrial zone." Atmospheric Research **96**(4): 612-625.

Atkinson, R. and A. C. Lloyd (1984). "Evaluation of Kinetic and Mechanistic Data for Modeling of Photochemical Smog." Journal of Physical and Chemical Reference Data **13**(2): 315-444.

AtmoHdF (2012). Inventaire régional des émissions de polluants atmosphériques, Atmo Hauts-de-France.

Badol, C., N. Locoge and J.-C. Galloo (2008). "Using a source-receptor approach to characterise VOC behaviour in a French urban area influenced by industrial emissions: Part II: Source contribution assessment using the Chemical Mass Balance (CMB) model." Science of The Total Environment **389**(2–3): 429-440.

Badol, C., N. Locoge, T. Léonardis and J.-C. Galloo (2008). "Using a source–receptor approach to characterise VOC behaviour in a French urban area influenced by industrial emissions Part I: Study area description, data set acquisition and qualitative data analysis of the data set." Science of The Total Environment **389**(2–3): 441-452.

Boichu, M., O. Favez, V. Riffault, J. E. Petit, Y. Zhang, C. Brogniez, J. Sciare, I. Chiapello, L. Clarisse, S. Zhang, N. Pujol-Söhne, E. Tison, H. Delbarre and P. Goloub (2019). "Large-scale particulate air pollution and chemical fingerprint of volcanic sulfate aerosols from the

2014–2015 Holuhraun flood lava eruption of Bárðarbunga volcano (Iceland)." Atmos. Chem. Phys. **19**(22): 14253-14287.

Bouwman, A. F., D. P. Van Vuuren, R. G. Derwent and M. Posch (2002). "A Global Analysis of Acidification and Eutrophication of Terrestrial Ecosystems." Water, Air, and Soil Pollution **141**(1): 349-382.

Budisulistiorini, S. H., K. Baumann, E. S. Edgerton, S. T. Bairai, S. Mueller, S. L. Shaw, E. M. Knipping, A. Gold and J. D. Surratt (2015). "Seasonal characterization of submicron aerosol chemical composition and organic aerosol sources in the southeastern United States: Atlanta, Georgia and Look Rock, Tennessee." Atmos. Chem. Phys. Discuss. **15**(16): 22379-22417.

Canagaratna, M. R., J. T. Jayne, J. L. Jimenez, J. D. Allan, M. R. Alfarra, Q. Zhang, T. B. Onasch, F. Drewnick, H. Coe, A. Middlebrook, A. Delia, L. R. Williams, A. M. Trimborn, M. J. Northway, P. F. DeCarlo, C. E. Kolb, P. Davidovits and D. R. Worsnop (2007). "Chemical and microphysical characterization of ambient aerosols with the aerodyne aerosol mass spectrometer." Mass Spectrometry Reviews **26**(2): 185-222.

Carbone, S., S. Saarikoski, A. Frey, F. Reyes, P. Reyes, M. Castillo, E. Gramsch, P. Oyola, J. Jayne, D. R. Worsnop and R. Hillamo (2013). "Chemical Characterization of Submicron Aerosol Particles in Santiago de Chile." Aerosol and Air Quality Research **13**.

Cazier, F., D. Dewaele, A. Delbende, H. Nouali, G. Garçon, A. Verdin, D. Courcot, S. Bouhsina and P. Shirali (2011). "Sampling analysis and characterization of particles in the atmosphere of rural, urban and industrial areas." Procedia Environmental Sciences **4**(0): 218-227.

CGDD (2014). Bilan de la qualité de l'air en France en 2013, Commissariat général au développement durable.

Chen, S., Y. Zhao and R. Zhang (2018). "Formation Mechanism of Atmospheric Ammonium Bisulfate: Hydrogen-Bond-Promoted Nearly Barrierless Reactions of SO3 with NH3 and H2O." **19**(8): 967-972.

Cohen, A. J., H. Ross Anderson, B. Ostro, K. D. Pandey, M. Krzyzanowski, N. Kunzli, K. Gutschmidt, A. Pope, I. Romieu, J. M. Samet and K. Smith (2005). "The global burden of disease due to outdoor air pollution." J Toxicol Environ Health A **68**(13-14): 1301-1307.

Crenn, V., A. Chakraborty, I. Fronval, D. Petitprez and V. Riffault (2018). "Fine particles sampled at an urban background site and an industrialized coastal site in Northern France—Part 2: Comparison of offline and online analyses for carbonaceous aerosols." Aerosol Science and Technology **52**(3): 287-299.

Crenn, V., I. Fronval, D. Petitprez and V. Riffault (2017). "Fine particles sampled at an urban background site and an industrialized coastal site in Northern France - Part 1: Seasonal variations and chemical characterization." Sci Total Environ **578**: 203-218.

Crenn, V., J. Sciare, P. L. Croteau, S. Verlhac, R. Fröhlich, C. A. Belis, W. Aas, M. Äijälä, A. Alastuey, B. Artiñano, D. Baisnée, N. Bonnaire, M. Bressi, M. Canagaratna, F. Canonaco, C. Carbone, F. Cavalli, E. Coz, M. J. Cubison, J. K. Esser-Gietl, D. C. Green, V. Gros, L. Heikkinen, H. Herrmann, C. Lunder, M. C. Minguillón, G. Močnik, C. D. O'Dowd, J. Ovadnevaite, J. E. Petit, E. Petralia, L. Poulain, M. Priestman, V. Riffault, A. Ripoll, R. Sarda-Estève, J. G. Slowik, A. Setyan, A. Wiedensohler, U. Baltensperger, A. S. H. Prévôt, J. T. Jayne and O. Favez (2015). "ACTRIS ACSM intercomparison – Part 1: Reproducibility of concentration and fragment results from 13 individual Quadrupole Aerosol Chemical

626 Speciation Monitors (Q-ACSM) and consistency with co-located instruments." Atmos. Meas.
627 Tech. **8**(12): 5063-5087.

628 DeCarlo, P. F., J. R. Kimmel, A. Trimborn, M. J. Northway, J. T. Jayne, A. C. Aiken, M.
629 Gonin, K. Fuhrer, T. Horvath, K. S. Docherty, D. R. Worsnop and J. L. Jimenez (2006).
630 "Field-Deployable, High-Resolution, Time-of-Flight Aerosol Mass Spectrometer." Analytical
631 Chemistry **78**(24): 8281-8289.

632 DREAL (2012). Industrie au regard de l'environnement, Direction régionale de
633 l'environnement de l'aménagement et du logement Nord-Pas-de-Calais**:** 11-25.

634 Du, W., Y. L. Sun, Y. S. Xu, Q. Jiang, Q. Q. Wang, W. Yang, F. Wang, Z. P. Bai, X. D. Zhao
635 and Y. C. Yang (2015). "Chemical characterization of submicron aerosol and particle growth
636 events at a national background site (3295 m a.s.l.) on the Tibetan Plateau." Atmos. Chem.
637 Phys. **15**(18): 10811-10824.

638 Eatough, D. J., F. M. Caka and R. J. Farber (1994). "The Conversion of SO2 to Sulfate in the
639 Atmosphere." Israel Journal of Chemistry **34**(3-4): 301-314.

640 EEA (2015). Sector share for emissions of primary PM2.5 and PM10 particulate matter,
641 European Environment Agency**:** http://www.eea.europa.eu/data-and-maps/daviz/sector-split-
642 of-emissions-of-4#tab-chart_1.

643 El Haddad, I., B. D'Anna, B. Temime-Roussel, M. Nicolas, A. Boreave, O. Favez, D. Voisin,
644 J. Sciare, C. George, J. L. Jaffrezo, H. Wortham and N. Marchand (2013). "Towards a better
645 understanding of the origins, chemical composition and aging of oxygenated organic aerosols:
646 case study of a Mediterranean industrialized environment, Marseille." Atmos. Chem. Phys.
647 **13**(15): 7875-7894.

648 Elder, A., S. Vidyasagar and L. DeLouise (2009). "Physicochemical factors that affect metal
649 and metal oxide nanoparticle passage across epithelial barriers." Wiley Interdisciplinary
650 Reviews: Nanomedicine and Nanobiotechnology **1**(4): 434-450.

651 Flossmann, A. I., W. D. Hall and H. R. Pruppacher (1985). "A Theoretical Study of the Wet
652 Removal of Atmospheric Pollutants. Part I: The Redistribution of Aerosol Particles Captured
653 through Nucleation and Impaction Scavenging by Growing Cloud Drops." Journal of the
654 Atmospheric Sciences **42**(6): 583-606.

655 Ghan, S. J. and S. E. Schwartz (2007). "Aerosol Properties and Processes: A Path from Field
656 and Laboratory Measurements to Global Climate Models." Bulletin of the American
657 Meteorological Society **88**(7): 1059-1083.

658 Guo, H., L. Xu, A. Bougiatioti, K. M. Cerully, S. L. Capps, J. R. Hite Jr, A. G. Carlton, S. H.
659 Lee, M. H. Bergin, N. L. Ng, A. Nenes and R. J. Weber (2015). "Fine-particle water and pH
660 in the southeastern United States." Atmos. Chem. Phys. **15**(9): 5211-5228.

661 Heikkinen, L., M. Äijälä, M. Riva, K. Luoma, K. Dällenbach, J. Aalto, P. Aalto, D. Aliaga,
662 M. Aurela, H. Keskinen, U. Makkonen, P. Rantala, M. Kulmala, T. Petäjä, D. Worsnop and
663 M. Ehn (2020). "Long-term sub-micrometer aerosol chemical composition in the boreal
664 forest: inter- and intra-annual variability." Atmos. Chem. Phys. **20**(5): 3151-3180.

665 Hleis, D., I. Fernández-Olmo, F. Ledoux, A. Kfoury, L. Courcot, T. Desmonts and D. Courcot
666 (2013). "Chemical profile identification of fugitive and confined particle emissions from an
667 integrated iron and steelmaking plant." Journal of Hazardous Materials **250–251**: 246-255.

668 Jacob, D. J. and M. R. Hoffmann (1983). "A dynamic model for the production of H+ NO3−,
669 and SO42− in urban fog." Journal of Geophysical Research: Oceans **88**(C11): 6611-6621.

Jayne, J. T., D. C. Leard, X. Zhang, P. Davidovits, K. A. Smith, C. E. Kolb and D. R. Worsnop (2000). "Development of an Aerosol Mass Spectrometer for Size and Composition Analysis of Submicron Particles." Aerosol Science and Technology **33**(1-2): 49-70.

Jimenez, J. L., M. R. Canagaratna, N. M. Donahue, A. S. H. Prevot, Q. Zhang, J. H. Kroll, P. F. DeCarlo, J. D. Allan, H. Coe, N. L. Ng, A. C. Aiken, K. S. Docherty, I. M. Ulbrich, A. P. Grieshop, A. L. Robinson, J. Duplissy, J. D. Smith, K. R. Wilson, V. A. Lanz, C. Hueglin, Y. L. Sun, J. Tian, A. Laaksonen, T. Raatikainen, J. Rautiainen, P. Vaattovaara, M. Ehn, M. Kulmala, J. M. Tomlinson, D. R. Collins, M. J. Cubison, E., J. Dunlea, J. A. Huffman, T. B. Onasch, M. R. Alfarra, P. I. Williams, K. Bower, Y. Kondo, J. Schneider, F. Drewnick, S. Borrmann, S. Weimer, K. Demerjian, D. Salcedo, L. Cottrell, R. Griffin, A. Takami, T. Miyoshi, S. Hatakeyama, A. Shimono, J. Y. Sun, Y. M. Zhang, K. Dzepina, J. R. Kimmel, D. Sueper, J. T. Jayne, S. C. Herndon, A. M. Trimborn, L. R. Williams, E. C. Wood, A. M. Middlebrook, C. E. Kolb, U. Baltensperger and D. R. Worsnop (2009). "Evolution of Organic Aerosols in the Atmosphere." Science **326**(5959): 1525-1529.

Jimenez, J. L., J. T. Jayne, Q. Shi, C. E. Kolb, D. R. Worsnop, I. Yourshaw, J. H. Seinfeld, R. C. Flagan, X. Zhang, K. A. Smith, J. W. Morris and P. Davidovits (2003). "Ambient aerosol sampling using the Aerodyne Aerosol Mass Spectrometer." Journal of Geophysical Research: Atmospheres **108**(D7).

Kelly, F. J. and J. C. Fussell (2012). "Size, source and chemical composition as determinants of toxicity attributable to ambient particulate matter." Atmospheric Environment **60**: 504-526.

Khoder, M. I. (2002). "Atmospheric conversion of sulfur dioxide to particulate sulfate and nitrogen dioxide to particulate nitrate and gaseous nitric acid in an urban area." Chemosphere **49**(6): 675-684.

Kulmala, M., L. Pirjola and J. M. Makela (2000). "Stable sulphate clusters as a source of new atmospheric particles." Nature **404**(6773): 66-69.

Leclercq, B., A. Platel, S. Antherieu, L. Y. Alleman, E. M. Hardy, E. Perdrix, N. Grova, V. Riffault, B. M. Appenzeller, M. Happillon, F. Nesslany, P. Coddeville, J. M. Lo-Guidice and G. Garcon (2017). "Genetic and epigenetic alterations in normal and sensitive COPD-diseased human bronchial epithelial cells repeatedly exposed to air pollution-derived PM2.5." Environ Pollut **230**: 163-177.

Lei, L., C. Xie, D. Wang, Y. He, Q. Wang, W. Zhou, W. Hu, P. Fu, Y. Chen, X. Pan, Z. Wang, D. R. Worsnop and Y. Sun (2020). "Fine particle characterization in a coastal city in China: composition, sources, and impacts of industrial emissions." Atmos. Chem. Phys. **20**(5): 2877-2890.

Matsumoto, K. and H. Tanaka (1996). "Formation and dissociation of atmospheric particulate nitrate and chloride: An approach based on phase equilibrium." Atmospheric Environment **30**(4): 639-648.

Matthew, B. M., A. M. Middlebrook and T. B. Onasch (2008). "Collection Efficiencies in an Aerodyne Aerosol Mass Spectrometer as a Function of Particle Phase for Laboratory Generated Aerosols." Aerosol Science and Technology **42**(11): 884-898.

Mazzarella, G., V. Esposito, A. Bianco, F. Ferraraccio, M. V. Prati, A. Lucariello, L. Manente, A. Mezzogiorno and A. De Luca (2012). "Inflammatory effects on human lung epithelial cells after exposure to diesel exhaust micron sub particles (PM1.0) and pollen allergens." Environmental Pollution **161**: 64-69.

Mbengue, S., L. Y. Alleman and P. Flament (2014). "Size-distributed metallic elements in submicronic and ultrafine atmospheric particles from urban and industrial areas in northern France." Atmospheric Research **135–136**(0): 35-47.

Middlebrook, A. M., R. Bahreini, J. L. Jimenez and M. R. Canagaratna (2011). "Evaluation of Composition-Dependent Collection Efficiencies for the Aerodyne Aerosol Mass Spectrometer using Field Data." Aerosol Science and Technology **46**(3): 258-271.

Minguillón, M. C., A. Ripoll, N. Pérez, A. S. H. Prévôt, F. Canonaco, X. Querol and A. Alastuey (2015). "Chemical characterization of submicron regional background aerosols in the western Mediterranean using an Aerosol Chemical Speciation Monitor." Atmos. Chem. Phys. **15**(11): 6379-6391.

Ng, N. L., S. C. Herndon, A. Trimborn, M. R. Canagaratna, P. L. Croteau, T. B. Onasch, D. Sueper, D. R. Worsnop, Q. Zhang, Y. L. Sun and J. T. Jayne (2011). "An Aerosol Chemical Speciation Monitor (ACSM) for Routine Monitoring of the Composition and Mass Concentrations of Ambient Aerosol." Aerosol Science and Technology **45**(7): 780-794.

Niyogi, D., H.-I. Chang, V. K. Saxena, T. Holt, K. Alapaty, F. Booker, F. Chen, K. J. Davis, B. Holben, T. Matsui, T. Meyers, W. C. Oechel, R. A. Pielke, R. Wells, K. Wilson and Y. Xue (2004). "Direct observations of the effects of aerosol loading on net ecosystem CO2 exchanges over different landscapes." Geophysical Research Letters **31**(20): L20506.

Park, S. S., A. D. A. Hansen and S. Y. Cho (2010). "Measurement of real time black carbon for investigating spot loading effects of Aethalometer data." Atmospheric Environment **44**(11): 1449-1455.

Parworth, C., J. Fast, F. Mei, T. Shippert, C. Sivaraman, A. Tilp, T. Watson and Q. Zhang (2015). "Long-term measurements of submicrometer aerosol chemistry at the Southern Great Plains (SGP) using an Aerosol Chemical Speciation Monitor (ACSM)." Atmospheric Environment **106**: 43-55.

Pérez, N., J. Pey, X. Querol, A. Alastuey, J. M. López and M. Viana (2008). "Partitioning of major and trace components in PM10–PM2.5–PM1 at an urban site in Southern Europe." Atmospheric Environment **42**(8): 1677-1691.

Petit, J. E., O. Favez, A. Albinet and F. Canonaco (2017). "A user-friendly tool for comprehensive evaluation of the geographical origins of atmospheric pollution: Wind and trajectory analyses." Environmental Modelling & Software **88**: 183-187.

Petit, J. E., O. Favez, J. Sciare, V. Crenn, R. Sarda-Estève, N. Bonnaire, G. Močnik, J. C. Dupont, M. Haeffelin and E. Leoz-Garziandia (2015). "Two years of near real-time chemical composition of submicron aerosols in the region of Paris using an Aerosol Chemical Speciation Monitor (ACSM) and a multi-wavelength Aethalometer." Atmos. Chem. Phys. **15**(6): 2985-3005.

Petzold, A., C. Kopp and R. Niessner (1997). "The dependence of the specific attenuation cross-section on black carbon mass fraction and particle size." Atmospheric Environment **31**(5): 661-672.

Pope, C. A., R. T. Burnett, M. J. Thun and et al. (2002). "Lung cancer, cardiopulmonary mortality, and long-term exposure to fine particulate air pollution." JAMA **287**(9): 1132-1141.

Ramgolam, K., O. Favez, H. Cachier, A. Gaudichet, F. Marano, L. Martinon and A. Baeza-Squiban (2009). "Size-partitioning of an urban aerosol to identify particle determinants involved in the proinflammatory response induced in airway epithelial cells." Part Fibre Toxicol **6**: 10.

Riffault, V., J. Arndt, H. Marris, S. Mbengue, A. Setyan, L. Y. Alleman, K. Deboudt, P. Flament, P. Augustin, H. Delbarre and J. Wenger (2015). "Fine and Ultrafine Particles in the Vicinity of Industrial Activities: A Review." Critical Reviews in Environmental Science and Technology: 1-52.

Rimetz-Planchon, J., E. Perdrix, S. Sobanska and C. Brémard (2008). "PM10 air quality variations in an urbanized and industrialized harbor." Atmospheric Environment **42**(31): 7274-7283.

Ripoll, A., M. C. Minguillón, J. Pey, J. L. Jimenez, D. A. Day, Y. Sosedova, F. Canonaco, A. S. H. Prévôt, X. Querol and A. Alastuey (2015). "Long-term real-time chemical characterization of submicron aerosols at Montsec (southern Pyrenees, 1570 m a.s.l.)." Atmos. Chem. Phys. **15**(6): 2935-2951.

Rivellini, L. H., I. Chiapello, E. Tison, M. Fourmentin, A. Féron, A. Diallo, T. N'Diaye, P. Goloub, F. Canonaco, A. S. H. Prévôt and V. Riffault (2017). "Chemical characterization and source apportionment of submicron aerosols measured in Senegal during the 2015 SHADOW campaign." Atmos. Chem. Phys. **17**(17): 10291-10314.

Roig Rodelas, R., E. Perdrix, B. Herbin and V. Riffault (2019). "Characterization and variability of inorganic aerosols and their gaseous precursors at a suburban site in northern France over one year (2015–2016)." Atmospheric Environment **200**: 142-157.

Roukos, J., V. Riffault, N. Locoge and H. Plaisance (2009). "VOC in an urban and industrial harbor on the French North Sea coast during two contrasted meteorological situations." Environmental Pollution **157**(11): 3001-3009.

Schlag, P., A. Kiendler-Scharr, M. J. Blom, F. Canonaco, J. S. Henzing, M. M. Moerman, A. S. H. Prévôt and R. Holzinger (2015). "Aerosol source apportionment from 1 year measurements at the CESAR tower at Cabauw, NL." Atmos. Chem. Phys. Discuss. **2015**: 35117-35155.

Schwartz, S. E. (1987). Aqueous-Phase Reactions in Clouds. The Chemistry of Acid Rain, American Chemical Society. **349:** 93-108.

Setyan, A., P. Flament, N. Locoge, K. Deboudt, V. Riffault, L. Y. Alleman, C. Schoemaecker, J. Arndt, P. Augustin, R. M. Healy, J. C. Wenger, F. Cazier, H. Delbarre, D. Dewaele, P. Dewalle, M. Fourmentin, P. Genevray, C. Gengembre, T. Leonardis, H. Marris and S. Mbengue (2019). "Investigation on the near-field evolution of industrial plumes from metalworking activities." Science of The Total Environment **668**: 443-456.

Stavroulas, I., A. Bougiatioti, G. Grivas, D. Paraskevopoulou, M. Tsagkaraki, P. Zarmpas, E. Liakakou, E. Gerasopoulos and N. Mihalopoulos (2019). "Sources and processes that control the submicron organic aerosol composition in an urban Mediterranean environment (Athens): a high temporal-resolution chemical composition measurement study." Atmos. Chem. Phys. **19**(2): 901-919.

Stein, A. F., R. R. Draxler, G. D. Rolph, B. J. B. Stunder, M. D. Cohen and F. Ngan (2016). "NOAA's HYSPLIT Atmospheric Transport and Dispersion Modeling System." Bulletin of the American Meteorological Society **96**(12): 2059-2077.

Stockwell, W. R. and J. G. Calvert (1983). "The mechanism of the HO-SO2 reaction." Atmospheric Environment (1967) **17**(11): 2231-2235.

Sun, Y., Z. Wang, H. Dong, T. Yang, J. Li, X. Pan, P. Chen and J. T. Jayne (2012). "Characterization of summer organic and inorganic aerosols in Beijing, China with an Aerosol Chemical Speciation Monitor." Atmospheric Environment **51**: 250-259.

Sun, Y., Z. Wang, P. Fu, Q. Jiang, T. Yang, J. Li and X. Ge (2013). "The impact of relative humidity on aerosol composition and evolution processes during wintertime in Beijing, China." Atmospheric Environment **77**: 927-934.

Taiwo, A. M., R. M. Harrison, D. C. S. Beddows and Z. Shi (2014). "Source apportionment of single particles sampled at the industrially polluted town of Port Talbot, United Kingdom by ATOFMS." Atmospheric Environment **97**: 155-165.

Taiwo, A. M., R. M. Harrison and Z. Shi (2014). "A review of receptor modelling of industrially emitted particulate matter." Atmospheric Environment **97**: 109-120.

Takahama, S., A. Johnson, J. Guzman Morales, L. M. Russell, R. Duran, G. Rodriguez, J. Zheng, R. Zhang, D. Toom-Sauntry and W. R. Leaitch (2013). "Submicron organic aerosol in Tijuana, Mexico, from local and Southern California sources during the CalMex campaign." Atmospheric Environment **70**: 500-512.

Tiitta, P., V. Vakkari, P. Croteau, J. P. Beukes, P. G. van Zyl, M. Josipovic, A. D. Venter, K. Jaars, J. J. Pienaar, N. L. Ng, M. R. Canagaratna, J. T. Jayne, V. M. Kerminen, H. Kokkola, M. Kulmala, A. Laaksonen, D. R. Worsnop and L. Laakso (2014). "Chemical composition, main sources and temporal variability of PM1 aerosols in southern African grassland." Atmos. Chem. Phys. **14**(4): 1909-1927.

Virkkula, A., T. Mäkelä, R. Hillamo, T. Yli-tuomi, A. Hirsikko, K. Hameri and I. k. Koponen (2007). "A simple procedure for correcting loading effects of aethalometer data." Journal of the Air & Waste Management Association **57**(10).

von der Weiden, S. L., F. Drewnick and S. Borrmann (2009). "Particle Loss Calculator – a new software tool for the assessment of the performance of aerosol inlet systems." Atmos. Meas. Tech. **2**(2): 479-494.

Weber, R. J., G. Chen, D. D. Davis, R. L. Mauldin, D. J. Tanner, F. L. Eisele, A. D. Clarke, D. C. Thornton and A. R. Bandy (2001). "Measurements of enhanced H2SO4 and 3–4 nm particles near a frontal cloud during the First Aerosol Characterization Experiment (ACE 1)." Journal of Geophysical Research: Atmospheres **106**(D20): 24107-24117.

Weingartner, E., H. Saathoff, M. Schnaiter, N. Streit, B. Bitnar and U. Baltensperger (2003). "Absorption of light by soot particles: determination of the absorption coefficient by means of aethalometers." Journal of Aerosol Science **34**(10): 1445-1463.

West, J. J., A. S. Ansari and S. N. Pandis (1999). "Marginal PM25: Nonlinear Aerosol Mass Response to Sulfate Reductions in the Eastern United States." Journal of the Air & Waste Management Association **49**(12): 1415-1424.

WHO (2002). The world health report 2002 - Reducing Risks, Promoting Healthy Life. Geneva**:** http://www.who.int/whr/2002/en/whr2002_en.pdf?ua=2001.

Xiang, Y., H. Delbarre, S. Sauvage, T. Léonardis, M. Fourmentin, P. Augustin and N. Locoge (2012). "Development of a methodology examining the behaviours of VOCs source apportionment with micro-meteorology analysis in an urban and industrial area." Environmental Pollution **162**: 15-28.

Zhang, Q., M. R. Canagaratna, J. T. Jayne, D. R. Worsnop and J.-L. Jimenez (2005). "Time- and size-resolved chemical composition of submicron particles in Pittsburgh: Implications for aerosol sources and processes." Journal of Geophysical Research: Atmospheres **110**(D7): D07S09.

Zhang, Q., J. L. Jimenez, M. R. Canagaratna, J. D. Allan, H. Coe, I. Ulbrich, M. R. Alfarra, A. Takami, A. M. Middlebrook, Y. L. Sun, K. Dzepina, E. Dunlea, K. Docherty, P. F.

DeCarlo, D. Salcedo, T. Onasch, J. T. Jayne, T. Miyoshi, A. Shimono, S. Hatakeyama, N. Takegawa, Y. Kondo, J. Schneider, F. Drewnick, S. Borrmann, S. Weimer, K. Demerjian, P. Williams, K. Bower, R. Bahreini, L. Cottrell, R. J. Griffin, J. Rautiainen, J. Y. Sun, Y. M. Zhang and D. R. Worsnop (2007). "Ubiquity and dominance of oxygenated species in organic aerosols in anthropogenically-influenced Northern Hemisphere midlatitudes." Geophysical Research Letters **34**(13): L13801.

Zhang, Q., J. L. Jimenez, D. R. Worsnop and M. Canagaratna (2007). "A Case Study of Urban Particle Acidity and Its Influence on Secondary Organic Aerosol." Environmental Science & Technology **41**(9): 3213-3219.

Zhao, Y., Y. Liu, J. Ma, Q. Ma and H. He (2017). "Heterogeneous reaction of SO2 with soot: The roles of relative humidity and surface composition of soot in surface sulfate formation." Atmospheric Environment **152**: 465-476.

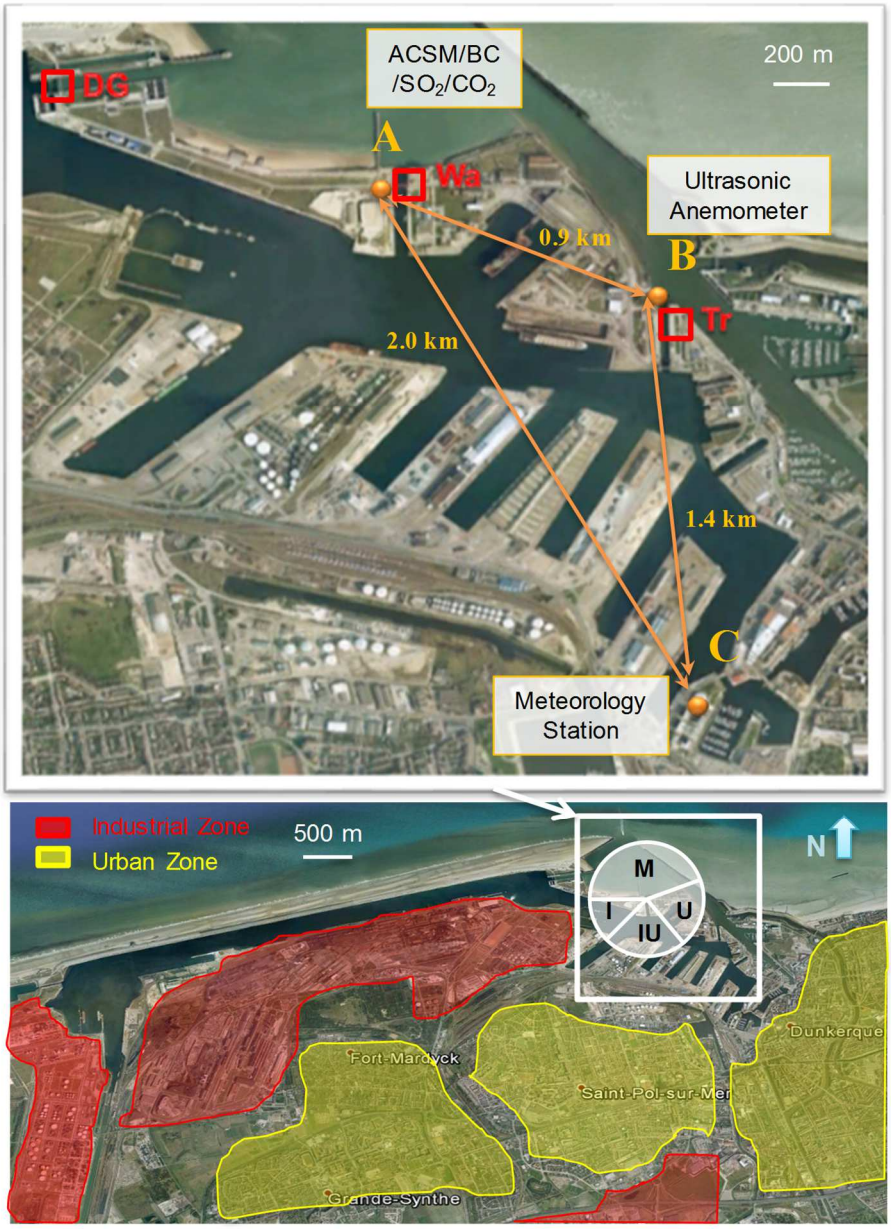

Figure 1. (Bottom) Maps of the urban-industrial area of Dunkirk (M: marine, U: urban, IU: industrial-urban, I: industrial wind sectors); Top Locations of the measurements: (A) Port-Est: ACSM and other chemical measurements; (B) Ultrasonic anemometer; (C) Meteorology station. Locks indicated in red (DG: De Gaulle; Wa: Watier; Tr: Trystram) (adapted from Google Maps)

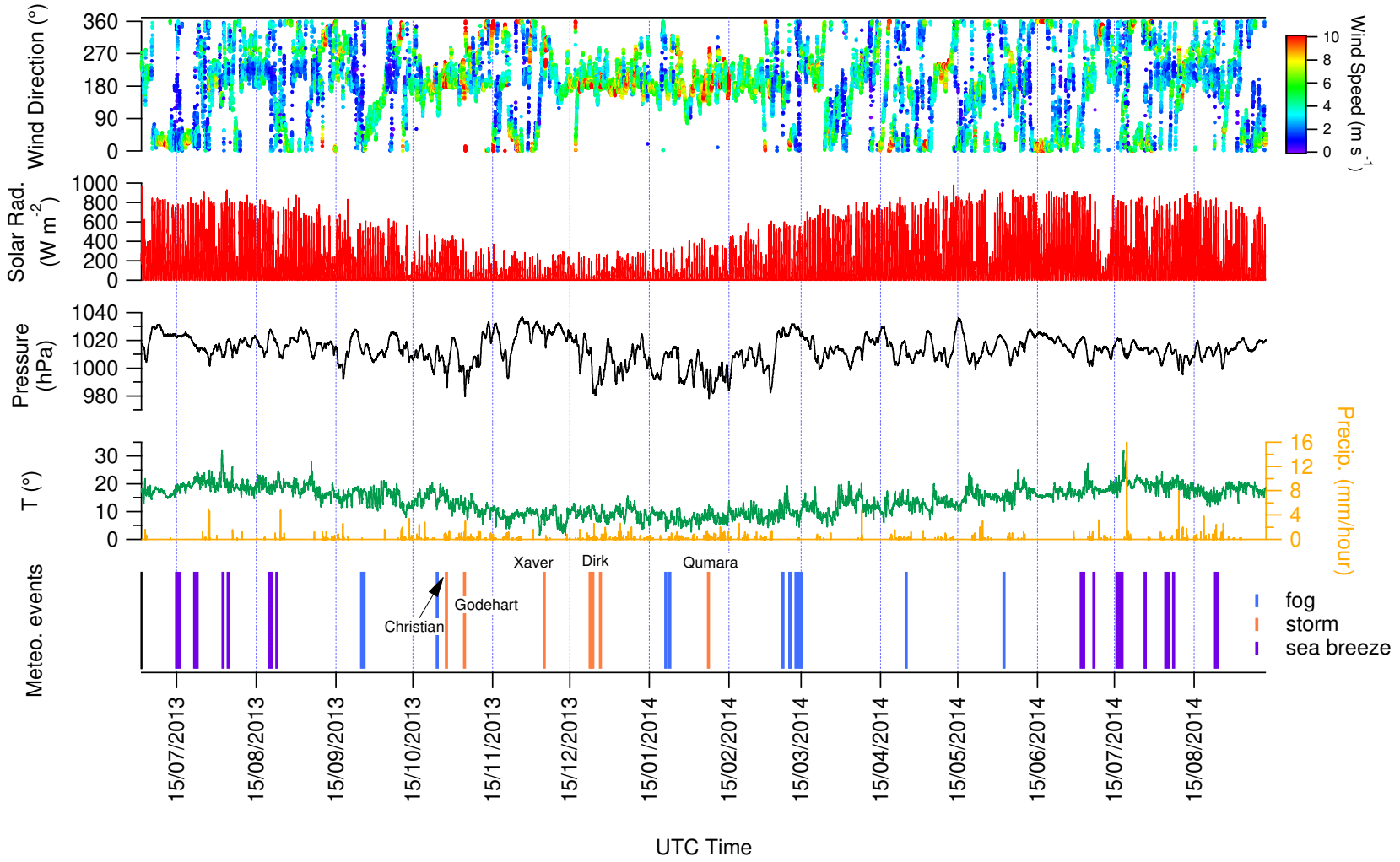

Figure 2. From top to bottom: wind direction colored by wind speed, solar radiation, pressure, temperature and precipitation, and identified meteorological events (fog, storm and sea breeze).

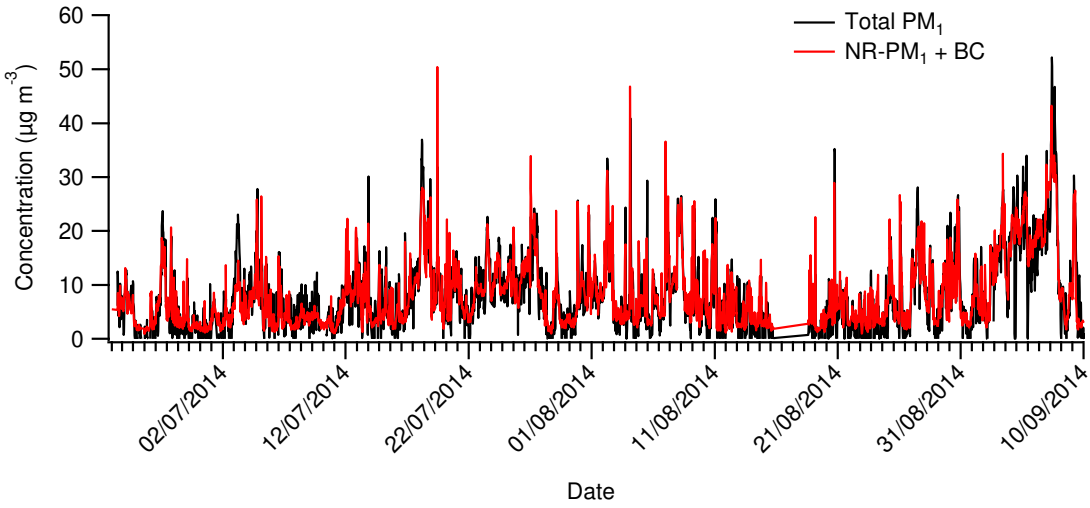

(a)

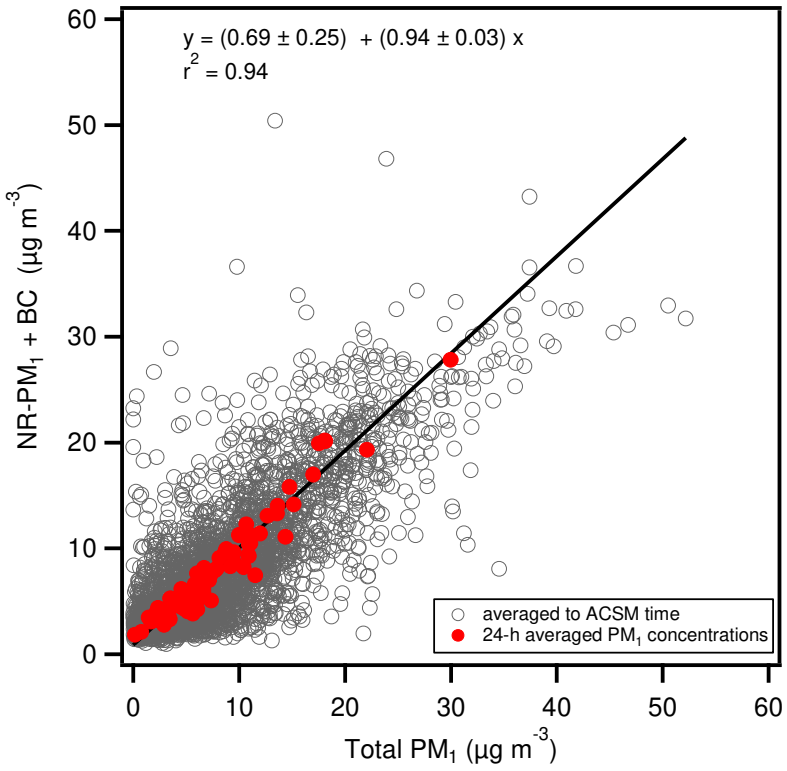

(b)

Figure 3. (a) Time series of NR-PM_1+BC measured by ACSM+aethalometer vs. Total PM_1 measured by TEOM-FDMS; (b) Scatter plot of PM_1 concentrations (NR-PM_1+BC vs. Total PM_1): averaged to ACSM time (grey) and 24-h averaged concentration (red). Linear fit performed on 24-h averaged values.

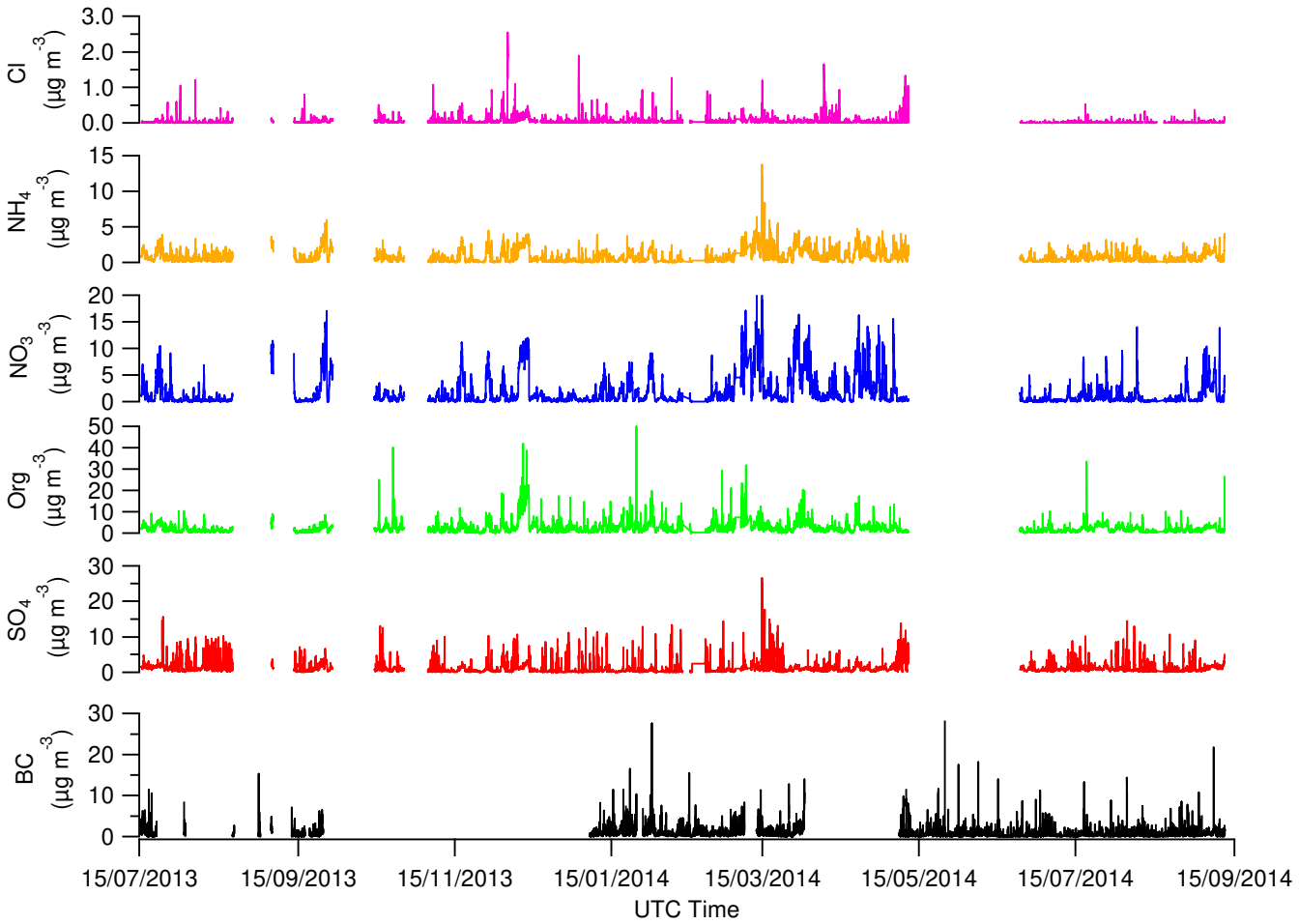

876

877 Figure 4. Time series of the chemical composition of NR-PM_1 measured by ACSM (Cl, SO_4, NH_4, NO_3, and Org), and Black carbon measured

878 by aethalometer.

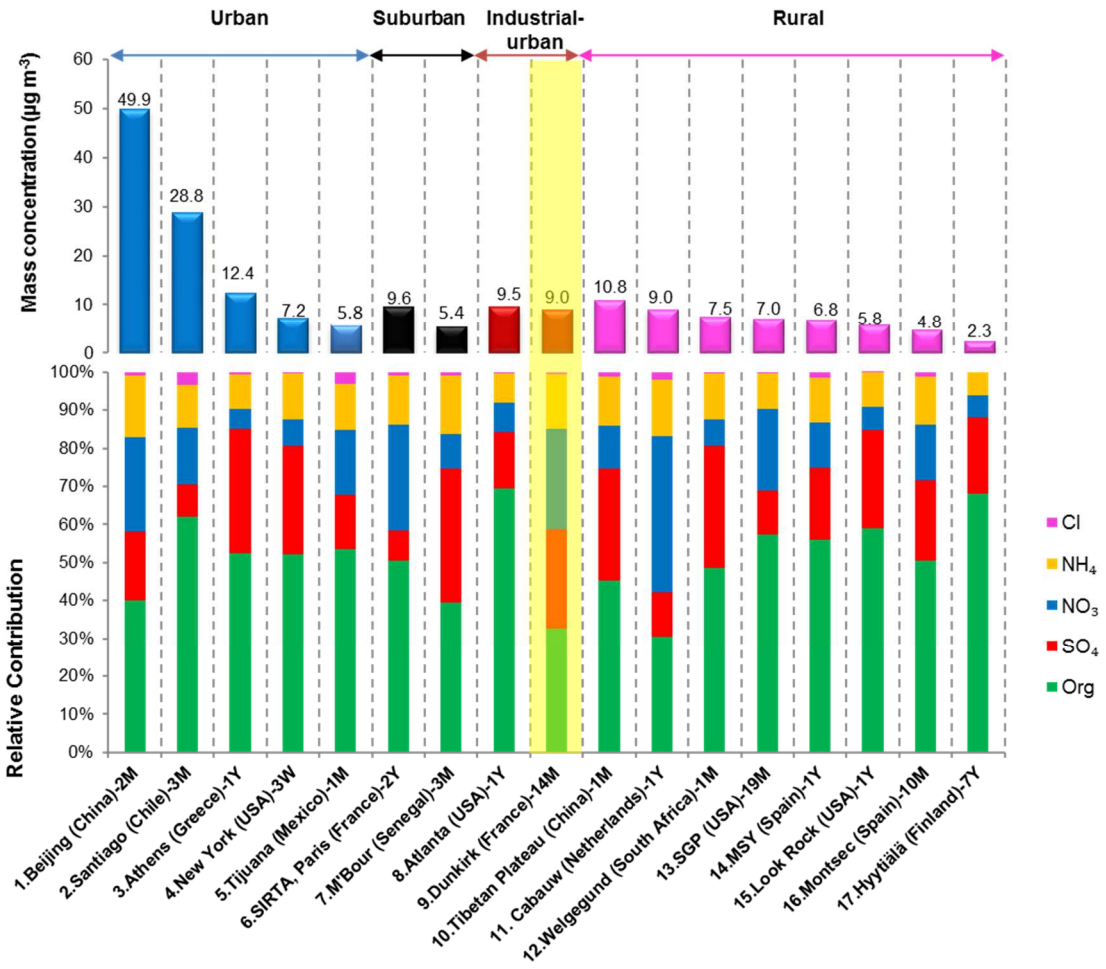

Figure 5. Comparison of averaged concentrations and chemical compositions of NR-PM_1 for this study and other ACSM field campaigns. Details on the location and duration of each campaign are given on the horizontal axis (M: months; W: weeks; Y: year). SGP: Southern Great Plains, MSY: Montseny.

1. Beijing (China) (Sun et al. 2012); 2. Santiago (Chile) (Carbone et al. 2013); 3. Athens (Greece) (Stavroulas et al. 2019); 4. New York (USA) (Ng et al. 2011); 5.Tijuana (Mexico) (Takahama et al. 2013); 6. SIRTA, Paris (France) (Petit et al. 2015); 7. M'Bour (Senegal) (Rivellini et al. 2017); 8.&15. Atlanta (USA) and Look Rock (USA) (Budisulistiorini et al. 2015); 9. This study; 10. Tibetan Plateau (China) (Du et al. 2015); 11. Cabauw (Netherlands)(Schlag et al. 2015); 12. Welgegund (South Africa) (Tiitta et al. 2014); 13. SGP (USA)(Parworth et al. 2015); 14.SMY (Spain) (Minguillón et al. 2015); 16. Montsec (Spain) (Ripoll et al. 2015). 17. Hyytiälä (Finland) (Heikkinen et al. 2020)

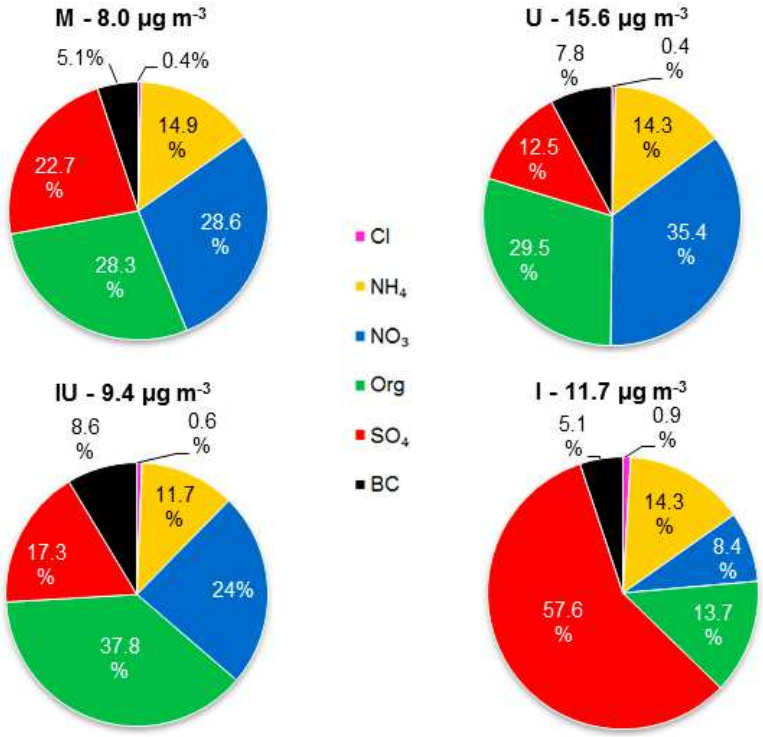

891 Figure 6. Chemical speciation of PM_1 for the four wind sectors (M: marine, U: urban, IU:
892 industrial-urban, I: industrial).

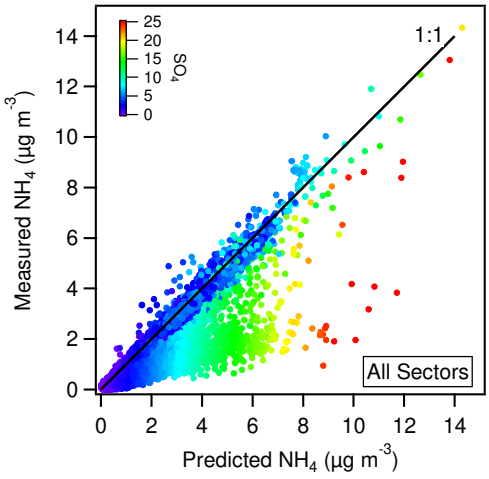

(a)

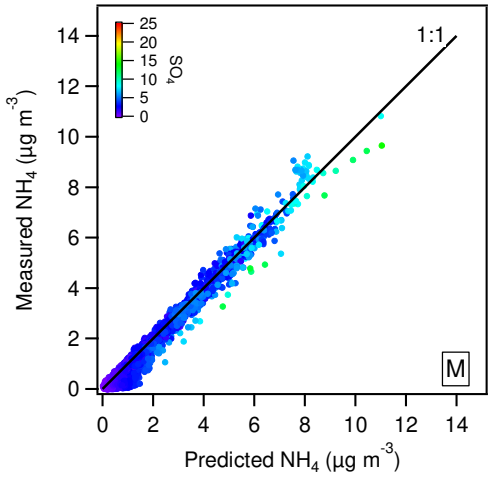

(b)

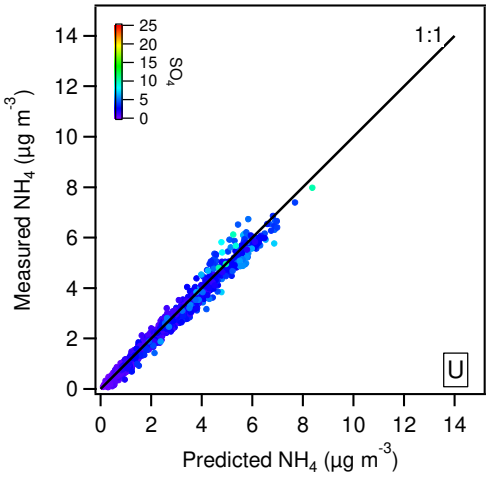

(c)

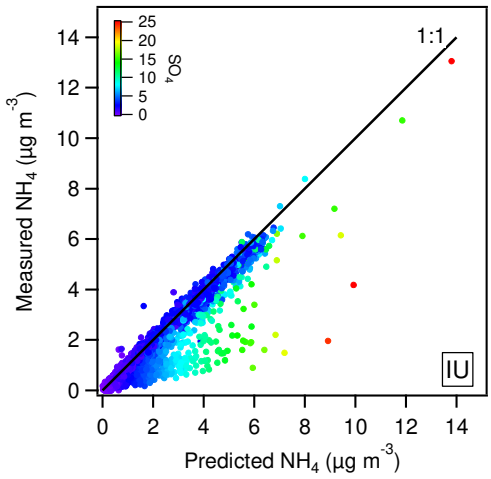

(d)

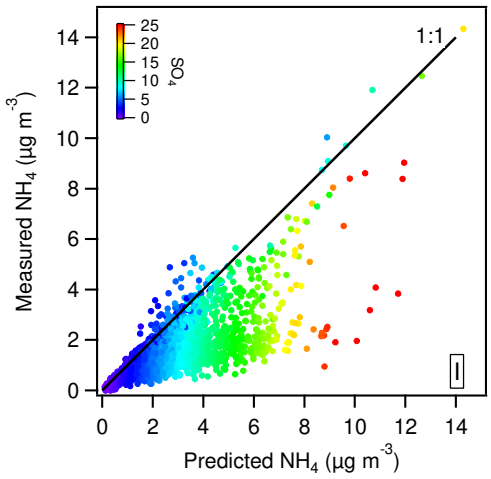

(e)

Figure 7. Correlation between measured and predicted NH_4 color coded by the sulfate concentration (µg m^{-3}) (a) for the entire study and (b) – (e) for marine (M), urban (U), industrial-urban (IU) and industrial (I) wind sectors, respectively. The black line represents the 1:1 line.

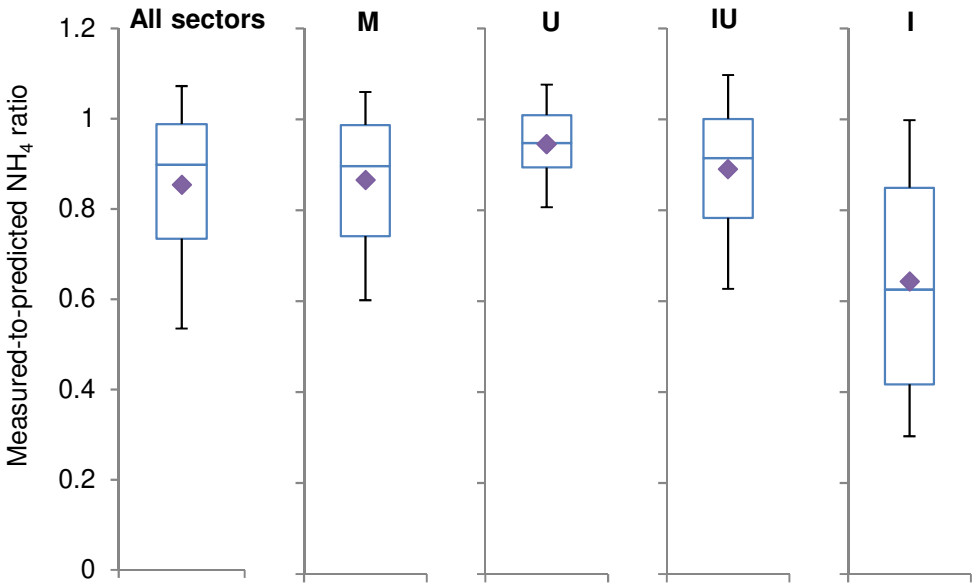

(a)

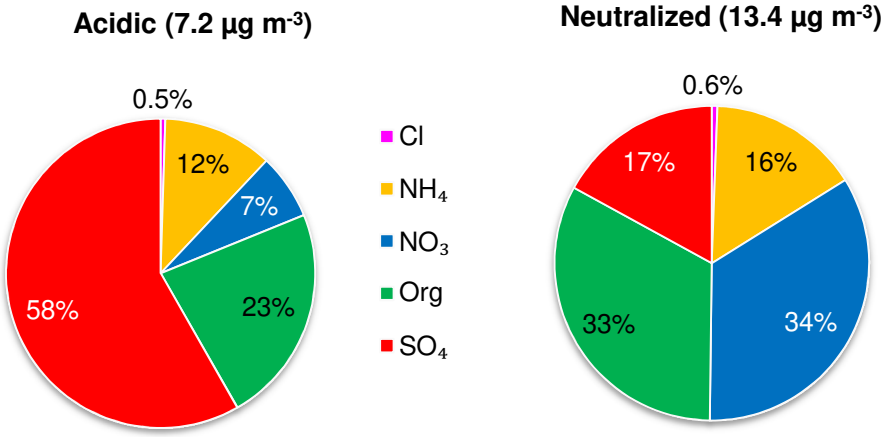

(b)

Figure 8. (a) Box plots of the measured-to-predicted NH_4 ratio for the entire study and the four wind sectors. The data correspond to the mean (diamond), median (horizontal line), 25th and 75th percentiles (lower and upper boxes), and 10th and 90th percentiles (lower and upper whiskers). (b) Chemical speciation of NR-PM_1 species for (left) acidic particles (measured-to-predicted ratio less than 0.75) and (right) neutralized particles (ratio between 0.85 − mean value − and 1.07 − 90th percentile).

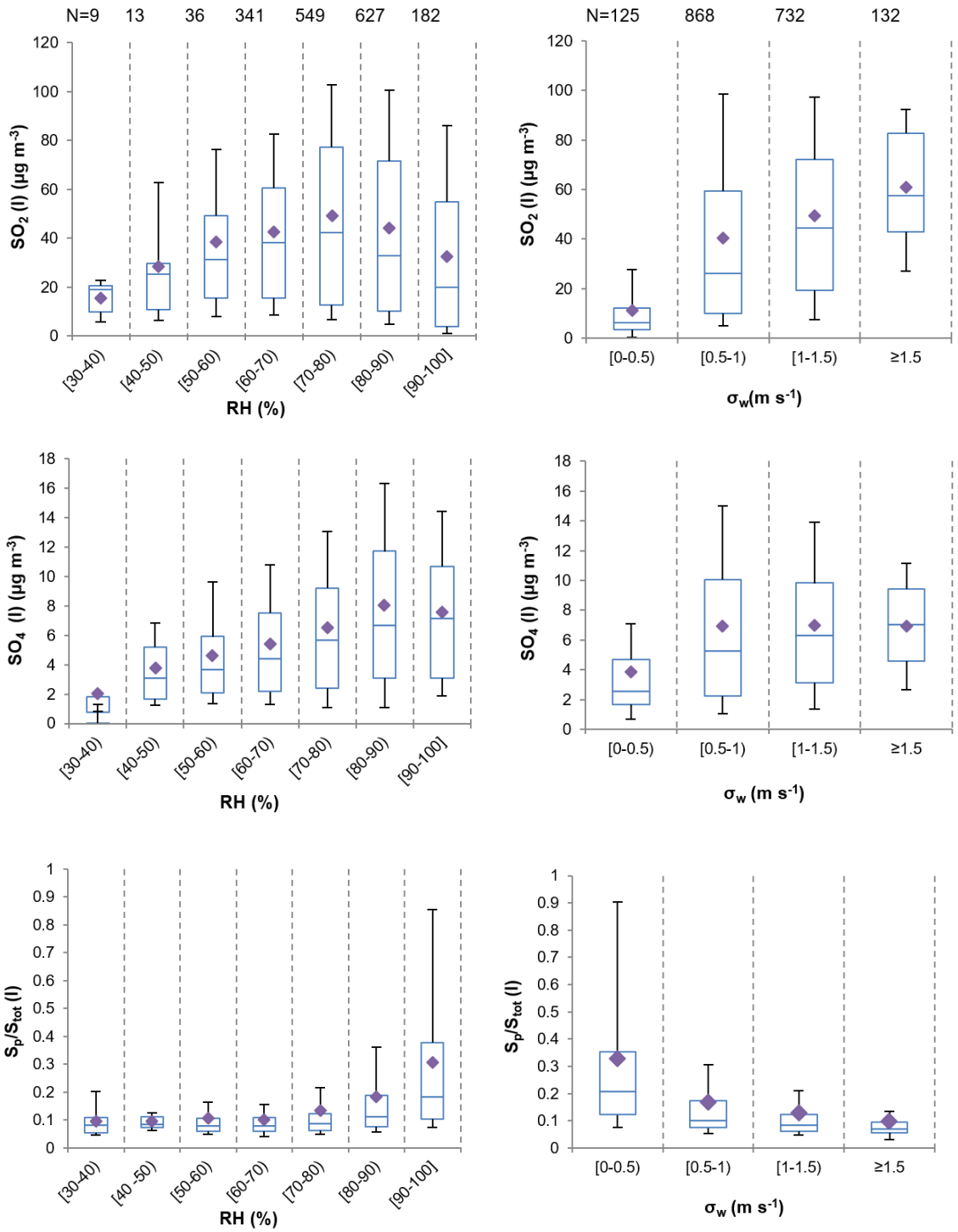

908 (a)

909 (b)

910 (c)

911 Figure 9. Dependences on relative humidity (left) and σ_w (right) of (a) SO_2, (b) SO_4 and (c)
912 the particulate-to-total sulfur ratio within the industrial (I) wind sector. The data correspond to
913 the mean (diamond), median (horizontal line), 25th and 75th percentiles (lower and upper
914 boxes), and 10th and 90th percentiles (lower and upper whiskers).

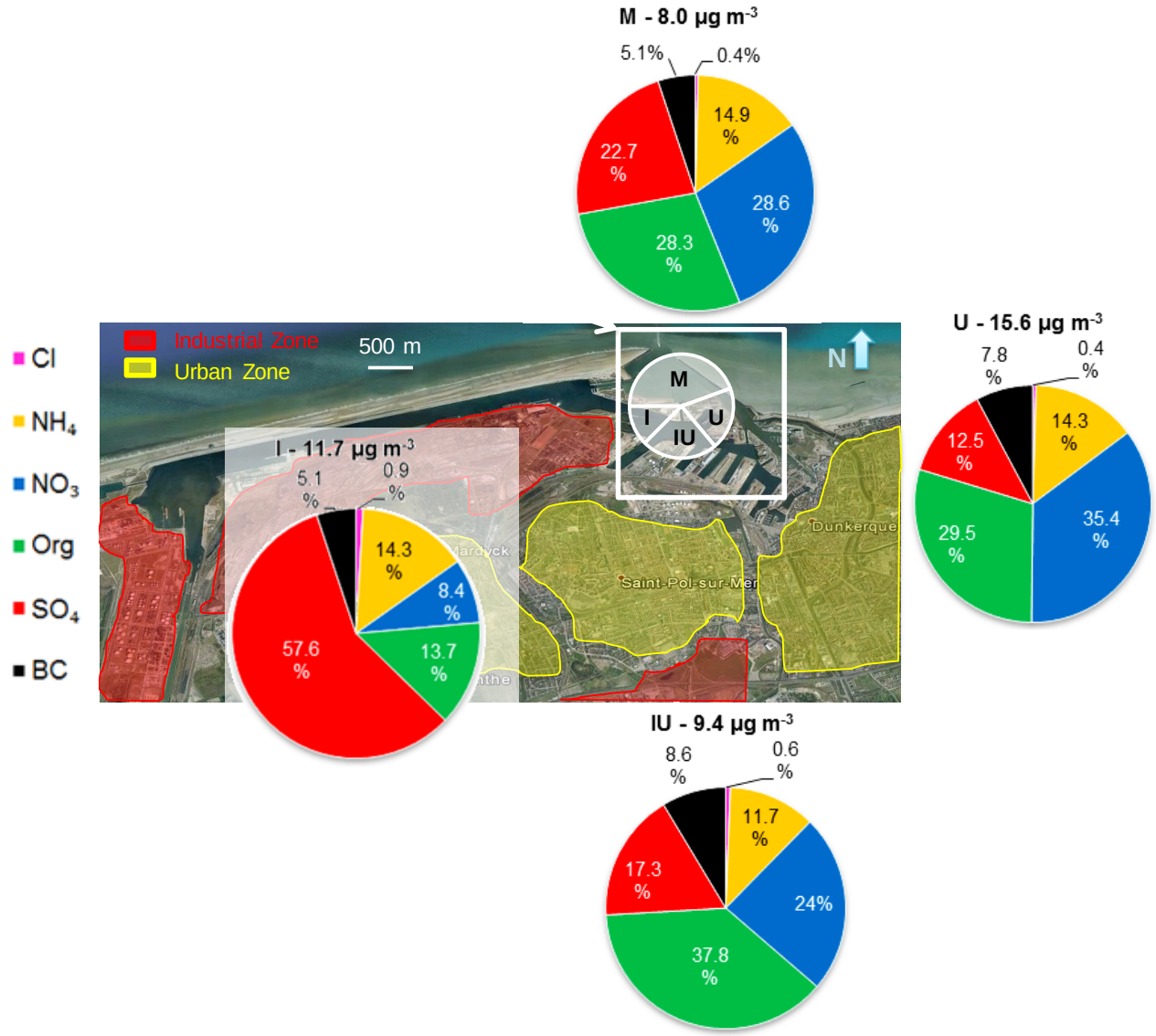
M - 8.0 µg m-3
5.1%
0.4%
14.9 %
22.7 %
28.6 %
28.3 %
U - 15.6 µg m-3
7.8 %
0.4 %
14.3 %
12.5 %
35.4 %
29.5 %
IU - 9.4 µg m-3
8.6 %
0.6 %
11.7 %
17.3 %
24%
37.8 %
I - 11.7 µg m-3
5.1 %
0.9 %
14.3 %
8.4 %
57.6 %
13.7 %
Cl
NH4
NO3
Org
SO4
BC
Industrial Zone
Urban Zone
500 m
N
M
I
U
IU
Dunkerque
Saint-Pol-sur-Mer